sustainability

Article

Decentralized Power Flow Control Strategy Using Transition Operations of DC-Bus Voltage for Detection of Uncertain DC Microgrid Operations

Muhammad Alif Miraj Jabbar, Dat Thanh Tran and Kyeong-Hwa Kim *

Department of Electrical and Information Engineering, Research Center for Electrical and Information Technology, Seoul National University of Science and Technology, 232 Gongneung-ro, Nowon-gu, Seoul 01811, Republic of Korea; alifmiraj@gmail.com (M.A.M.J.); tranthanhdat1506@gmail.com (D.T.T.)
* Correspondence: k2h1@seoultech.ac.kr; Tel.: +82-2-970-6406

Abstract: To enhance the reliability and flexibility of DC microgrids (DCMGs), this paper presents a decentralized power flow control strategy (PFCS) by using the transition operation modes. The transition operation modes are introduced as an effective communication method among power units, eliminating the use of additional digital communication links (DCLs) for the purpose of ensuring the power balance as well as the voltage regulation even under uncertain conditions. During the transition operation modes, the power unit which transmits the information shifts the DC-link voltage level, and the power unit which receives the information continuously monitors the DC-link voltage with predetermined time. When uncertain conditions occur in a particular power unit, this power unit triggers the transition operation modes to send this information to all power units in the DCMG system. The proposed PFCS can maintain the DC-link voltage at the nominal value for steady-state conditions both in the grid-connected mode and islanded mode. Moreover, the proposed PFCS significantly enhances the overall reliability of the decentralized DCMG system by effectively addressing several uncertainties stemmed from electricity price fluctuations, grid availability, battery state-of-charge (SOC) levels, and wind power variations. The scalability of the DCMG system is also demonstrated by incorporating an electric vehicle (EV) unit as an additional energy storage system (ESS). The EV unit seamlessly cooperates with the existing battery unit, functioning as additional ESS to regulate the DC-link voltage when the battery SOC level is low. Simulation and experimentation results under various conditions demonstrate the effectiveness of the proposed PFCS.

Keywords: DC microgrid; decentralized control architecture; detection of uncertain microgrid operations; power flow control; transition mode operations

check for updates

Citation: Jabbar, M.A.M.; Tran, D.T.; Kim, K.-H. Decentralized Power Flow Control Strategy Using Transition Operations of DC-Bus Voltage for Detection of Uncertain DC Microgrid Operations. *Sustainability* **2023**, *15*, 11635. https://doi.org/10.3390/su151511635

Academic Editors: Qian Xiao, Yiqi Liu, Jun Zeng and Fei Gao

Received: 6 July 2023
Revised: 20 July 2023
Accepted: 26 July 2023
Published: 27 July 2023

1. Introduction

The global energy infrastructure is undergoing a transformation, driven by the need for sustainable and resilient power systems. As traditional centralized power generation models face challenges of efficiency, reliability, and environmental impact, the demand for decentralized energy solutions attracts worldwide attention from researchers. In this context, microgrids have emerged as a promising concept that offers a new paradigm for efficient and flexible power distribution and management. A microgrid, defined as a localized and self-contained power system, provides a reliable and resilient electricity supply. In general, the microgrid integrates various distributed energy resources (DERs), renewable energy, energy storage systems (ESSs), and controllable loads [1]. As the world's energy situation keeps changing, microgrids are becoming increasingly important in driving the shift toward a sustainable and reliable energy future.

In the microgrid system, the DC microgrid (DCMG) has gained significant attention as a promising solution to realize efficient and sustainable power distribution systems. The DCMG system offers several advantages over the AC microgrid system because the issue regarding the synchronization of distributed generators, inrush currents caused by transformers, reactive power flow, harmonic currents, and three-phase unbalance does not exist in the DCMG system [2–4]. Furthermore, DCMG offers easy integration for DC energy sources such as photovoltaics (PV), fuel cells, and ESSs like batteries or supercapacitors [5,6].

In general, the DCMG system operation can be categorized into two modes: the grid-connected mode and islanded mode, depending on the availability of the main grid [7]. In the grid-connected mode, the utility grid primarily coordinates the exchange power in the DCMG to achieve power balance as well as voltage regulation. On the other hand, in the islanded mode, the power balance of the DCMG is maintained through a coordinated operation of specific power units, such as distributed generators (DGs) and ESSs. In the grid-connected mode, optimizing the cost of power consumption in a DCMG is a significant concern. Various methods such as time-of-use pricing (TOU), real-time pricing (RTP), and stepwise power tariff (SPT) are used worldwide to calculate electricity bills [8–11]. To optimize the power consumption cost of a DCMG system, previous studies have considered the electricity price change of the utility grid [12–14].

In terms of communication links, the DCMG control methods can be categorized as centralized control, distributed control, and decentralized control. The centralized control uses a central controller to determine the proper operation modes of each power unit by communicating with all power units through digital communication links (DCLs) [15]. In contrast, the distributed control also utilizes DCLs to collect data from adjacent power units without using the central controller. In this approach, each power unit independently determines its operation mode by considering data collected from its surroundings [16]. On the other hand, the decentralized control operates without the use of DCLs. In this scheme, the DCMG system autonomously maintains power balance by relying solely on local measurements of each unit [17,18]. The absence of DCLs in the decentralized control eliminates communication delays and simplifies system installation, thereby enhancing the system's scalability and flexibility [19]. The elimination of DCLs also has other potential benefits such as lower implementation costs and less dependency on communication systems, which can increase overall reliability and robustness [19–21]. Furthermore, the DCMG's vulnerability to cybersecurity threats may also be decreased, and the effort for maintenance and troubleshooting is reduced, which can potentially lead to faster problem resolution [21,22].

In a decentralized control scheme, the operation modes of each power unit in a DCMG system are determined using the DC-link voltage as a key indicator [23]. When there is surplus power in the DCMG, the DC-link voltage increases. On the contrary, a deficit of power in the DCMG leads to a decrease in the DC-link voltage. To enable power sharing among power sources in the DCMG system, voltage-based droop control methods have been introduced in the study [24]. These methods present the implementation of a virtual resistor to achieve the power balance of each converter in the DCMG system. Voltage/current (V/I) or voltage/power (V/P) characteristics are commonly used in the droop control method for the decentralized DCMG to achieve not only voltage regulation but also power balance [25].

Despite the effective power-sharing characteristic of the droop control, it still has the drawback of DC-link voltage deviation [26]. This deviation in DC-link voltage impacts the delivered power to the load. A significant deviation affects power accuracy, while even a slight deviation may influence power-sharing precision [27]. To overcome this issue, a voltage restoration scheme for a decentralized DCMG is presented in [28], in which the DC-link voltage is maintained at a constant value by injecting or absorbing power. For optimal power-sharing, another study successfully implements the DC-link voltage controller in the centralized and distributed control schemes [29,30]. In these schemes, the DC-link voltage controller should be implemented by at least one power unit in every operation mode of the DCMG.

Aside from the DC voltage deviation, another concern for a reliable decentralized DCMG operation is to carefully manage the battery state-of-charge (SOC) level to avoid faster battery degradation [31]. It is imperative to ensure that the battery operates primarily at high SOC levels for the extension of its lifespan. In the study [32], the low SOC level is only used for certain emergency operations to increase the reliability of DCMG operations. In addition to the battery SOC management, the reliability of the DCMG can be further improved by separately considering the electrical loads as non-critical and critical loads with different priorities [33]. Numerous studies in the field of microgrids have emphasized the importance of maintaining critical loads as well as improving the resilience and survivability of critical loads [34]. Motivated by these concerns, the battery SOC levels will be categorized according to the respective significance in this paper. During periods of low SOC levels, only critical loads are supplied based on the given priority. In this case, non-critical loads are subject to load shedding to achieve high resilience and reliability for the microgrid operation.

To enhance the reliability and optimize the operation of a microgrid system, this paper presents a power flow control scheme (PFCS) for a decentralized DCMG system. The transition operation modes are utilized in the proposed scheme to transmit the information on the DCMG system to other power units without the use of additional DCLs. This is achieved by continuously monitoring the DC-link voltage value in all power units. The DCMG system considered in this study consists of a utility grid unit, battery unit, wind turbine unit, and load units. In the grid-connected mode, the DC-link voltage control method is employed by the utility grid unit. On the other hand, in the islanded mode, the battery and wind turbine units alternate the regulation of the DC-link voltage to the nominal value. In the proposed PFCS, various factors such as the generation power of the wind turbine unit, battery SOC level, grid availability, load demand, and electricity price conditions are considered to develop an overall control strategy for the decentralized DCMG system. In addition, the scalability issue of the DCMG system is also studied by considering an electric vehicle (EV) unit as an additional ESS in the DCMG system. The contribution of the proposed method is to enhance the reliability and optimize the operation of the DCMG system without using the DCLs for significantly reduced system price. The PFCS is proposed to achieve the optimum operating condition and maintain the DC link voltage at steady-state conditions. The DCMG system inevitably has uncertain conditions such as grid electricity price change, grid fault, battery SOC reaching emergency level, or variation of wind power generation. To deal with such uncertain conditions effectively without DCLs, the transition mode operations are used in the proposed scheme for the purpose of detecting the uncertainties in the DCMG operation and changing the operations of power units accordingly.

The simulation is carried out to verify the effectiveness of the proposed decentralized control scheme by using the Powersim (PSIM) software (9.1, Powersim, Rockville, MD, USA). The simulation results confirm the effectiveness of the proposed approach in achieving optimal power-sharing, even in the presence of diverse conditions such as fluctuations in electricity prices, grid availability, uncertainties in battery SOC in the islanded mode, wind power variation, and EV unit involvement. The experimental results are also presented to support the simulation results by using a prototype DCMG test setup. The main contributions of this paper are summarized as follows:

(i) The proposed PFCS for a decentralized DCMG is capable of maintaining the DC-link voltage at the nominal value for steady-state conditions both in the grid-connected mode and islanded mode. In addition, the proposed PFCS autonomously changes the DCMG operation to guarantee the power balance even in the presence of uncertain DCMG conditions such as electricity price changes, grid availability, battery SOC level, wind power variation, and EV unit involvement.

(ii) In the proposed PFCS for a decentralized DCMG, the transition operation modes are introduced as an effective way to communicate between power units without the use of additional DCLs for the purpose of ensuring the power balance as well as the voltage regulation even under uncertain conditions. During the transition operation modes, the power unit which transmits the information shifts the DC-link voltage level. Meanwhile, the power unit which receives the information continuously monitors the DC-link voltage with predetermined time. When an uncertain condition occurs in a particular power unit, it uses the transition operation modes to send this information to all power units in the DCMG system. After this uncertain condition is acknowledged by all power units, the DCMG operation is switched back from the transition operation mode to the optimum steady-state operation.

(iii) The proposed PFCS improves the reliability of the DCMG system by carefully managing the battery SOC level. Furthermore, the proposed PFCS allows the easy integration of an EV unit within the DCMG system as additional ESS to support the battery unit that functions as the primary ESS. When the battery SOC approaches a low level, the EV unit undertakes the DC-link voltage regulation to ensure the power balance.

This paper is organized as follows: Section 2 presents the system configuration of a decentralized DCMG system. Section 3 describes the proposed control strategy of a decentralized DCMG. Section 4 addresses the proposed PFCS of a decentralized DCMG. Sections 5 and 6 present the simulation and experimental results, respectively. Finally, Section 7 concludes the paper.

2. System Configuration of a Decentralized DCMG

2.1. Configuration of DCMG

The configuration of a decentralized DCMG system presented in this paper is illustrated in Figure 1, comprising four primary power units: a utility grid unit, a wind turbine unit, a battery unit, and a load unit. An EV unit can also be considered as an additional ESS.

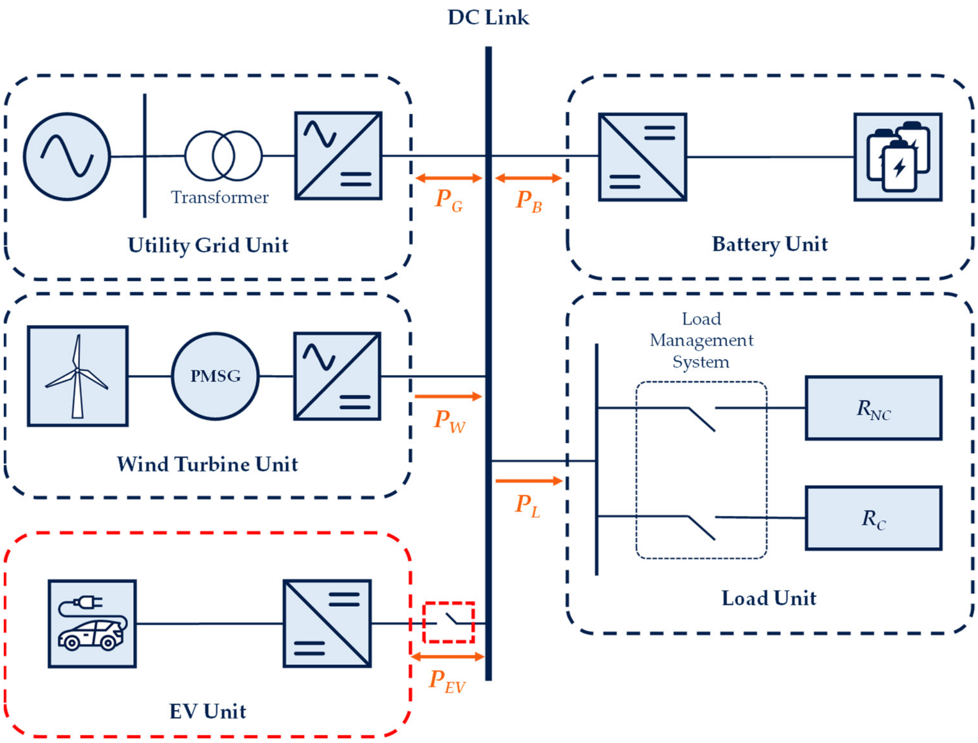

Figure 1. Configuration of a decentralized DCMG.

The utility grid unit connects the main grid to the DC-link through a transformer and a bidirectional AC/DC converter. The wind turbine unit uses a permanent magnet synchronous generator (PMSG) to convert mechanical power into electrical power, which is then fed into the DC-link through a unidirectional AC/DC converter. Both the battery unit and the EV unit utilize bidirectional interleaved DC/DC converters to exchange powers with the DC-link. The load unit which consists of critical load (R_C) and non-critical load (R_{NC}) employs electronic switches for load shedding and load reconnection.

In the DCMG system, several power units such as the utility grid, battery, and EV have bidirectional power flow, enabling them to either supply power into the DC-link, or absorb power from the DC-link. In contrast, the wind turbine unit only supplies power into the DC-link, and the load unit absorbs power from the DC-link. As shown in Figure 1, P_G, P_B, P_W, and P_L denote the power flow of the utility grid unit, the battery unit, the wind turbine unit, and the load unit, respectively. The power injection and current flow into the DC-link are represented as negative (−) values, while power absorption and current flow from the DC-link are represented as positive (+) values. The power of the EV unit (P_{EV}) functions similarly to the battery unit, serving as an additional ESS. The operational details and control methods of converters are determined by the proposed PFCS of the DCMG, which will be discussed in subsequent sections. The EV unit is dealt with separately from the proposed PFCS and functions as an additional plug-and-play ESS.

2.2. Management of Battery SOC

The management strategy of the battery SOC level used in the proposed decentralized PFCS of the DCMG system is shown in Figure 2. Battery operation is determined according to SOC levels and connected loads as specified in Table 1.

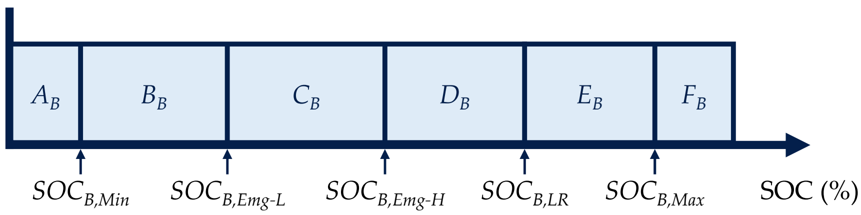

Figure 2. Battery operating states according to SOC level.

Table 1. SOC levels for battery unit.

SOC	Values	Purposes
$SOC_{B,Min}$	5%	Level to stop discharging in islanded mode
$SOC_{B,Emg\text{-}L}$	20%	Level to activate R_C load reconnection in islanded mode
$SOC_{B,Emg\text{-}H}$	25%	Level to activate R_{NC} load shedding in islanded mode
		Level to stop discharging in grid-connected mode with high electricity price condition
$SOC_{B,LR}$	50%	Level to activate R_{NC} load reconnection in islanded mode
$SOC_{B,Max}$	90%	Level to stop charging in both islanded and grid-connected modes

First, to prevent the critical situation, $SOC_{B,Min}$ is defined as 5%, which is the level to stop discharging in the islanded mode. At a battery SOC level lower than $SOC_{B,Min}$, the battery unit is always in charging mode. The second SOC level is $SOC_{B,Emg\text{-}L}$, at which the load reconnection process is activated for the critical load R_C. The third SOC level defined as $SOC_{B,Emg\text{-}H}$ is used for two purposes. This level is used to stop discharging the battery in grid-connected mode with high electricity price condition. It is also used to activate load shedding for the non-critical load R_{NC} in the islanded mode. The fourth SOC level is defined as $SOC_{B,LR}$ which is used to activate load reconnection for non-critical load R_{NC} if the battery unit has activated load shedding previously for R_{NC}. The last SOC level defined as $SOC_{B,Max}$ is used to stop charging in both islanded and grid-connected modes.

3. Proposed Control Strategy of Decentralized DCMG

3.1. Operation Modes of Utility Grid Unit

Figure 3 shows the operation modes of the utility grid unit which are composed of one steady-state mode and two transition modes. The first mode, denoted by Rd_{G1}, in Figure 3 represents the steady-state mode in which the DC-link voltage V_{dc} is always maintained at the nominal DC-link voltage V_{Nom}. In Rd_{G1} operation, the utility grid unit works in the region between $-P_G^{max}$ and P_G^{max} to supply power to the DC-link by rectifier (REC) mode, or to absorb power from the DC-link by inverter (INV) mode.

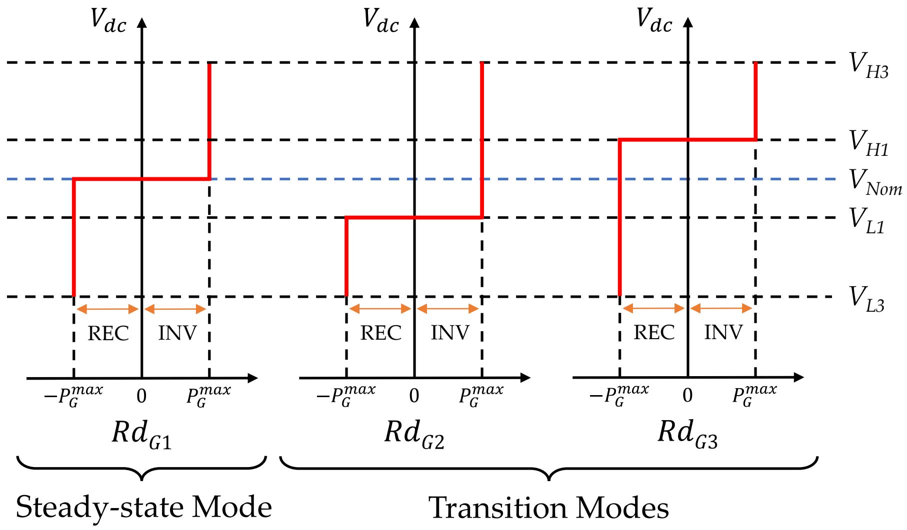

Figure 3. Operation modes of utility grid unit.

The second mode Rd_{G2}, is used during the transition period when the electricity price condition changes from normal to high. When this condition happens, the utility grid unit regulates V_{dc} to V_{L1} by adopting the Rd_{G2} mode in order that the battery unit identifies the electricity price condition change from normal to high by detecting the DC-link voltage variation. Then, the battery unit changes the operation in order to work properly under the high electricity price condition. After some predetermined time, the operation of the utility grid unit switches back to Rd_{G1} to maintain V_{dc} to V_{Nom}.

Another transition mode Rd_{G3} is used when the electricity price condition changes from high to normal, or when the grid is reconnected after a fault. Under these conditions, the utility grid unit temporarily changes from V_{dc} to V_{H1} by the Rd_{G3} mode for the purpose of transmitting this information to other power units. After some predetermined time, the operation of the utility grid unit is returned to steady-state mode Rd_{G1}.

3.2. Operation Modes of Battery Unit

The operation modes of the battery unit consist of five steady-state modes and four transition modes as illustrated in Figures 4 and 5. Figure 4 shows the steady-state operation modes of the battery unit which are separated into the operations in the grid-connected mode and islanded mode.

In steady-state grid-connected mode operation, the battery unit can work in the battery maximum current discharging mode (BDM) with Rd_{B1}, the battery maximum current charging mode (BCM) with Rd_{B2}, or idle mode with Rd_{B3}. In steady-state islanded mode operation, the battery unit can operate in BCM with Rd_{B2}, idle mode with Rd_{B3}, battery secondary voltage control discharging mode ($BVCM_{Dis}$) with Rd_{B4}, or battery secondary voltage control charging mode ($BVCM_{Cha}$) with Rd_{B5}. The Rd_{B1} mode is utilized in the grid-connected mode when the utility grid has high electricity price conditions. The Rd_{B2} mode is deployed either in the grid-connected mode with normal electricity price conditions, or in the islanded mode with the wind turbine unit regulating the DC-link voltage to V_{Nom}. The Rd_{B3} mode indicates the idle mode which is used when the battery SOC level reaches $SOC_{B,Max}$ in the charging condition, or when the battery SOC level falls to $SOC_{B,Emg\text{-}H}$ in the high electricity price condition. The Rd_{B4} and Rd_{B5} modes, which are only used in the islanded mode, implement $BVCM_{Dis}$ and $BVCM_{Cha}$. To regulate the DC-link voltage at

V_{Nom}, the operation of $BVCM_{Dis}$ and $BVCM_{Cha}$ is achieved by the primary droop control and secondary voltage control as shown in Figure 5. The Rd_{B4} mode is utilized when the generated power of the wind turbine unit is less than the demanded load in the islanded mode. In contrast, the Rd_{B5} mode is deployed to guarantee the DC-link voltage to V_{Nom} when the power of the wind turbine unit is in the region $[P_L, (P_L + P_B^{max})]$.

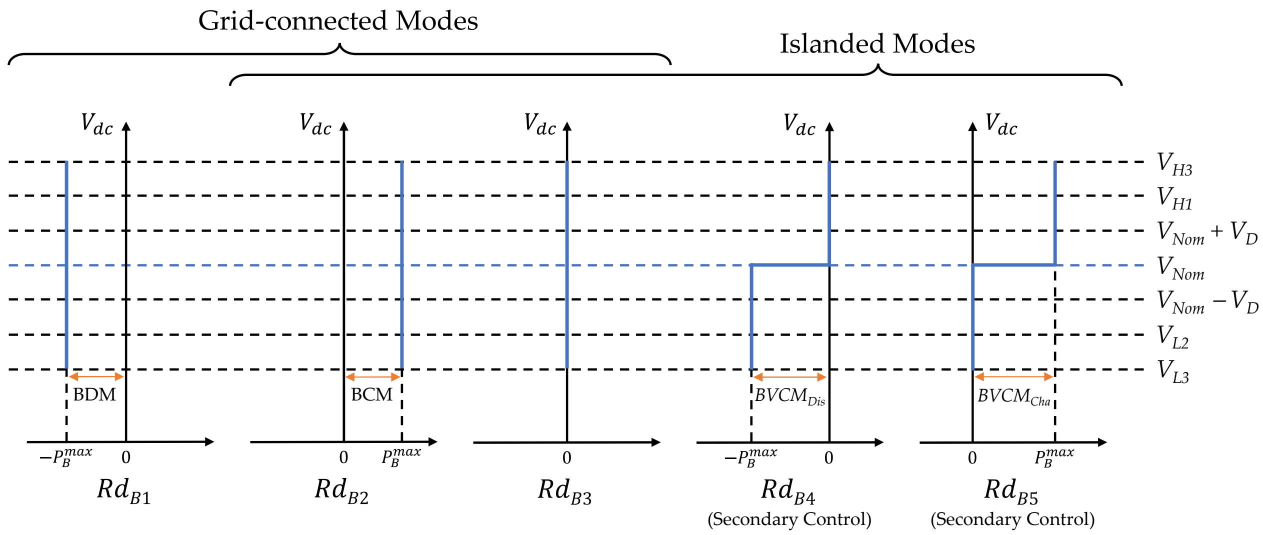

Figure 4. Steady-state operation modes of battery unit.

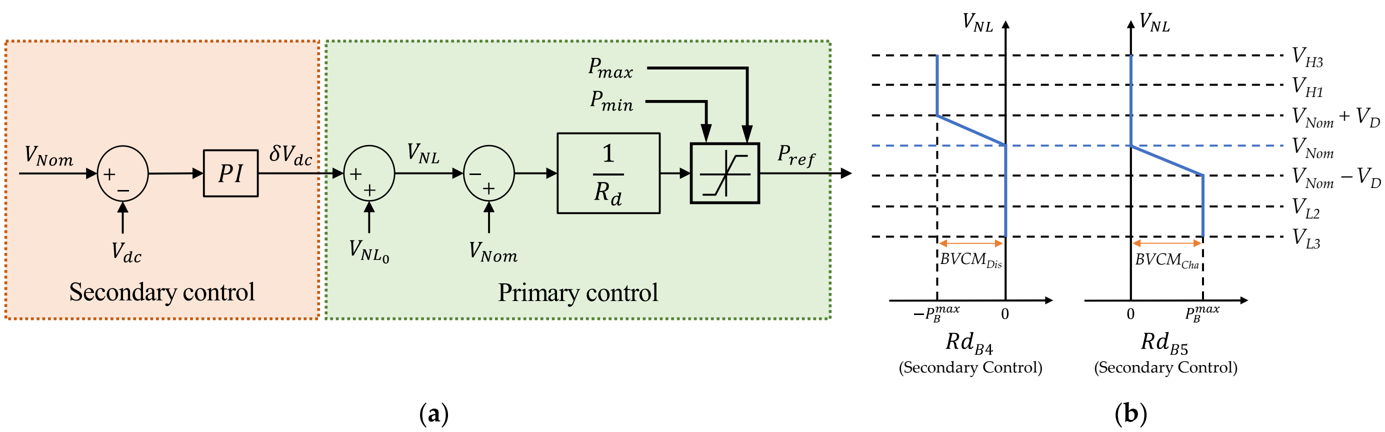

Figure 5. Secondary and primary controls to implement Rd_{B4} and Rd_{B5}. (**a**) Block diagram of the secondary control and primary control; (**b**) *V-P* droop curves ($V_{NL} - P_{ref}$).

Figure 5 shows the secondary and primary controls to implement Rd_{B4} and Rd_{B5}. The block diagram for the primary control and secondary control is shown in Figure 5a in which the primary control generates reference power (P_{ref}) to achieve power balance, and the secondary control regulates the DC-link voltage to V_{Nom}. In secondary control, the DC-link voltage is compared to the V_{Nom} and the error is fed to the proportional-integral (PI) controller. The PI controller output is added with the initial no-load voltage (V_{NL_0}) to produce a no-load voltage (V_{NL}) in the primary control. Finally, the V_{NL} is compared to the nominal voltage (V_{Nom}) to generate reference power (P_{ref}) by using the droop constant (R_d). Figure 5b shows the *V-P* droop curves for P_{ref} and V_{NL}.

Figure 6 shows the transition operation modes of the battery unit used only in the islanded mode. The first mode Rd_{B6} denotes the battery voltage control emergency mode ($BVCM_{Emg1}$) which is used to decrease the DC-link voltage to V_{L2} when the battery SOC level drops to $SOC_{B,Emg\text{-}H}$ in discharging. The Rd_{B6} mode is used to allow another ESS to respond to low DC-link voltage and to regulate DC-link voltage back to V_{Nom}. The second transition mode Rd_{B7} implements the battery voltage control emergency discharging mode ($BVCM_{Emg2,Dis}$) and battery voltage control emergency charging mode ($BVCM_{Emg2,Cha}$). These modes are used to maintain the DC-link voltage at V_{L2} after Rd_{B6} activation for R_{NC} load shedding in the islanded mode.

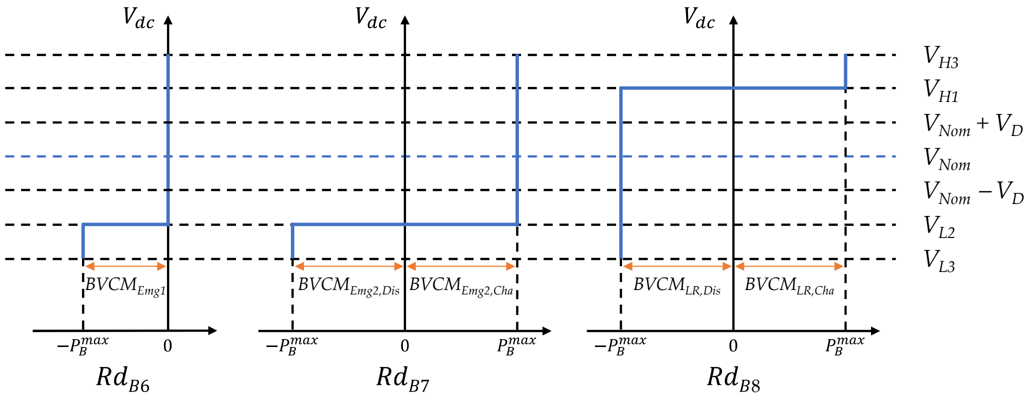

Figure 6. Transition operation modes of battery unit in islanded mode.

The last transition mode Rd_{B8} implements the battery voltage control load reconnection discharging mode ($BVCM_{LR,Dis}$) and battery voltage control load reconnection charging mode ($BVCM_{LR,Cha}$). These modes are deployed to increase the DC-link voltage at V_{H1} for load reconnection in the islanded mode. In the Rd_{B8} mode, the critical load R_C is reconnected as the battery SOC level reaches $SOC_{B,Emg\text{-}L}$. When the battery SOC level further increases to $SOC_{B,LR}$, the non-critical load R_{NC} is also reconnected.

3.3. Operation Modes of Wind Turbine Unit

Figure 7 shows the operation of the wind turbine unit which has two operation modes in steady-state and one operation mode in transient condition. The first mode, Rd_{W1}, denotes the wind voltage droop control mode (WVDCM) in the islanded mode during transition condition. In this mode, a primary droop control is utilized to reduce the wind power generation. The second mode, Rd_{W2} is a steady-state operation and happens when the wind turbine unit regulates the DC-link voltage in the islanded mode using wind voltage control mode (WVCM). When the absolute of the wind turbine power($|P_W|$) is higher than the sum of P_L and P_B^{max}, the WVCM mode uses a PI controller for DC-link voltage regulation. The third mode, Rd_{W3}, is the maximum power point tracking (MPPT) mode that is utilized to supply the maximum power to the DC-link either in the grid-connected mode or islanded mode.

3.4. Load Unit

The load unit consists of two categories of load, which are critical load (R_C) and non-critical load (R_{NC}). The total load (R_T) represents the case that both R_C and R_{NC} are connected. The load unit also detects the DC-link voltage for load shedding and load reconnection purposes. The details of the DC-link voltage detection are discussed in the next subsection.

3.5. Voltage Detection

In the proposed decentralized PFCS for a DCMG system, the power balance and voltage regulation are effectively achieved by detecting the DC-link voltage values without DCLs. All the power units can properly change the operation modes according to the DC-link voltage values after some predetermined time.

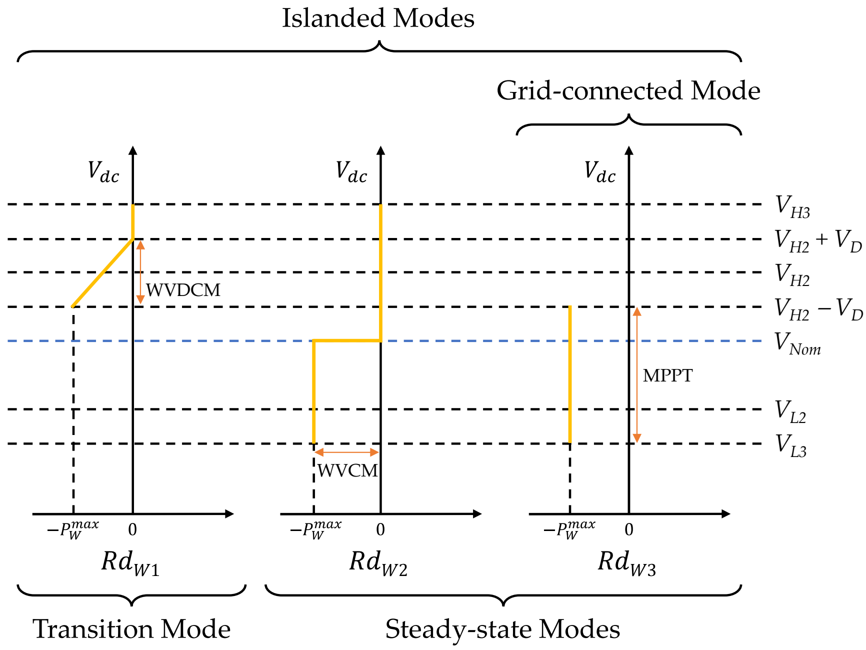

Figure 7. Operation modes of wind turbine unit.

Figure 8 shows the transition operation of DC-link voltage and information transmission in the case of $V_{dc} = V_{H1}$. Figure 8a shows the process of R_C reconnection in the islanded mode. As soon as the battery SOC level reaches $SOC_{B,Emg\text{-}L}$, the battery unit starts to operate with Rd_{B8} mode within 5 s to increase V_{dc} to V_{H1}. The load unit continuously monitors the V_{dc} level. Finally, if the V_{dc} value reaches V_{H1}, the load unit reconnects R_C after =3 s.

Figure 8b shows the process of R_{NC} reconnection in the islanded mode. As the battery SOC level reaches $SOC_{B,LR}$, the battery unit starts the Rd_{B8} mode within 10 s to increase the DC-link voltage to V_{H1}. The load unit continuously monitors whether the DC-link voltage V_{dc} is increased to V_{H1}. If the V_{dc} reaches to V_{H1}, the load unit reconnects R_{NC} after =8 s, resulting in the total load of R_T as shown in Figure 8b.

Figure 8c shows the process of the utility grid unit reconnection from fault in high electricity price condition. In this condition, the utility grid unit operates with Rd_{G3} to increase the DC-link voltage to V_{H1}. After 3 s, R_C is reconnected if R_C has been disconnected previously by load shedding. After 8 s, R_{NC} is reconnected if R_{NC} has been disconnected previously by load shedding. After 13 s, by observing the DC-link voltage value, the battery and the wind turbine units recognize that the utility grid is reconnected from the fault. Then, the wind turbine unit is returned to the MPPT mode to supply the maximum power to the DC-link. Depending on the SOC level, the battery unit works in BDM, BCM, or idle mode. After the transmission of the utility grid recovery information to other power units has been accomplished during 15 s, the utility grid unit returns to steady-state Rd_{G1} mode to regulate the DC-link voltage at V_{Nom}.

Figure 8d shows the process of the utility grid unit reconnection from fault in normal electricity price condition. Similar to Figure 8c, the utility grid unit operates with Rd_{G3} to increase the DC-link voltage to V_{H1}. If the load shedding has been activated previously, similar load reconnection is achieved after 3 s and 8 s, respectively. After 13 s, the wind turbine unit identifies the utility grid recovery, and starts the MPPT mode. It is worth mentioning that the wind turbine unit identifies only the utility grid recovery without having the exact information of the utility grid price condition. Only the battery unit recognizes the utility grid recovery as well as the normal electricity price condition after 18 s, if the Rd_{G3} operation by the utility grid unit lasts until 20 s. Then, the battery unit operates either in BCM or idle mode depending on the SOC level. Similarly, after the utility grid recovery information has been sent to other power units within 20 s, the utility grid unit changes the transition operation Rd_{G3} to steady-state operation Rd_{G1} to regulate the DC-link voltage at V_{Nom}.

Figure 8e shows the process of the utility grid unit electricity price change from high to normal. The utility grid unit operates with Rd_{G3} to increase the DC-link voltage to V_{H1}. After 18 s, the battery unit detects this voltage level to identify the electricity price change. Then, the battery unit changes the operation either in BCM or idle mode. Finally, after 20 s, the utility grid unit changes the operation to Rd_{G1} to regulate the DC-link voltage at V_{Nom} in the steady-state condition.

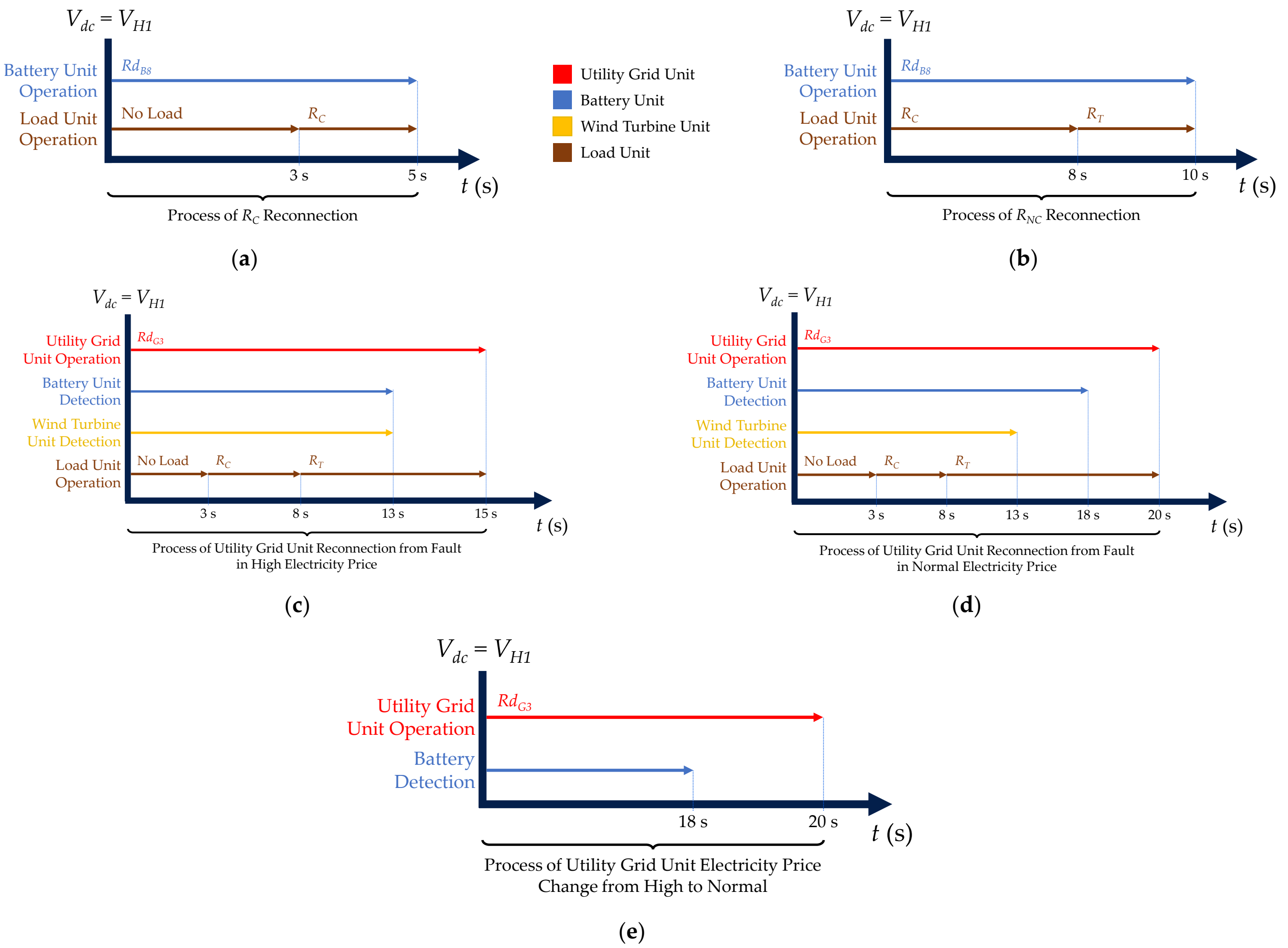

Figure 8. Transition operation of DC-link voltage and information transmission in case of V_{dc} = V_{H1}. (**a**) Process of R_C reconnection; (**b**) Process of R_{NC} reconnection; (**c**) Process of utility grid unit reconnection from fault in high electricity price condition; (**d**) Process of utility grid unit reconnection from fault in normal electricity price condition; (**e**) Process of utility grid unit electricity price change from high to normal.

Figure 9 shows the transition operation of DC-link voltage and information transmission in case of different values of V_{dc}. Figure 9a shows the process of the utility grid unit electricity price change from normal to high by using V_{dc} = V_{L1}. In this condition, the utility grid unit first operates in Rd_{G2} and decreases the DC-link voltage to V_{L1}. After 3 s, the battery unit acknowledges the electricity price condition change from normal to high by monitoring the V_{dc} level, and changes operation mode to BDM, idle, or BCM depending on the battery SOC level. After 5 s, the utility grid unit stops operating the Rd_{G2} and returns to steady-state operation mode Rd_{G1}.

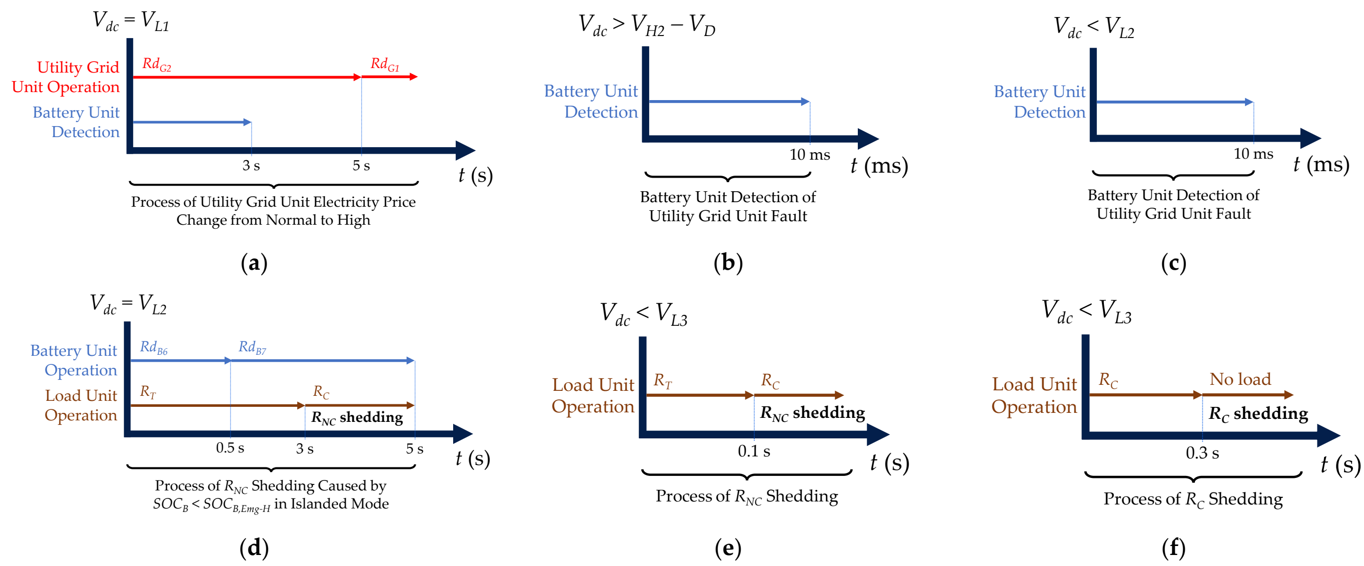

Figure 9. Transition operation of DC-link voltage and information transmission in case of different values of V_{dc}. (**a**) V_{dc} = V_{L1} for process of utility grid unit electricity price change from normal to high; (**b**) $V_{dc} > V_{H2} - V_D$ for process of utility grid fault; (**c**) $V_{dc} < V_{L2}$ for process of utility grid fault; (**d**) V_{dc} = V_{L2} for process of R_{NC} shedding caused by $SOC_B < SOC_{B,Emg\text{-}H}$ in islanded mode; (**e**) $V_{dc} < V_{L3}$ for process of R_{NC} shedding; (**f**) $V_{dc} < V_{L3}$ for process of R_C shedding.

Figure 9b,c show how the battery unit detects the utility grid unit fault with two different high-voltage and low-voltage conditions, respectively. If a fault occurs in the utility grid unit during INV mode operation, the DC-link voltage is rapidly increased. Figure 9b shows the detection process of the battery unit for this case. On the contrary, Figure 9c shows the detection process of the battery unit for grid fault with low voltage when the utility grid unit works in REC mode before the fault. If those DC-link voltage conditions last for 10 ms, the battery unit confirms the grid fault.

Figure 9d shows the process of R_{NC} load shedding in the islanded mode. As the battery unit SOC level reaches $SOC_{B,Emg\text{-}H}$ in the islanded mode, the battery unit changes operation to Rd_{B6} for $BVCM_{Emg1}$, and reduces the DC-link voltage to the second level of low DC-link voltage (V_{L2}). As soon as the DC-link voltage decreases to V_{L2}, the battery unit changes the operation to Rd_{B7} after 0.5 s, and the load unit activates load shedding for R_{NC} after 3 s.

Figure 9e,f show the process of load shedding for R_{NC} and R_C, respectively. Figure 9e shows the process of R_{NC} shedding after 0.1 s when the DC-link voltage drops to the third level of low DC-link voltage (V_{L3}). Figure 9f shows the process of R_C shedding after 0.3 s when the DC-link voltage falls to V_{L3}.

Figure 10 shows the transition operation of DC-link voltage and information transmission in the islanded mode the in case of $V_{dc} > V_{H2} - V_D$. Figure 10a shows the process of the battery unit operation change from $BVCM_{Dis}$ to $BVCM_{Cha}$ in case of $|P_W| > P_L$ in the islanded mode. When $|P_W|$ is higher than P_L, the wind turbine unit operates in WVDCM and V_{dc} increases to the value of $V_{H2} - V_D$. By detecting this increased voltage, the battery unit operation is changed from Rd_{B4} to Rd_{B5} after 1 s. Then, the wind turbine unit operates back in the MPPT mode as the battery unit regulates DC-link voltage in $BVCM_{Cha}$.

Figure 10b shows the process of the wind turbine unit regulating the DC-link voltage to V_{Nom}. When $|P_W|$ is higher than P_L even with battery charging operation, the wind turbine unit operates in WVDCM in Rd_{W1} and V_{dc} increases to the value of $V_{H2} - V_D$. Then, after 3 s, the battery unit changes the operation from $BVCM_{Cha}$ in Rd_{B5} to BCM in Rd_{B2}. After 5 s, the wind turbine unit changes operation from WVDCM in Rd_{W1} to WVCM in Rd_{W2}.

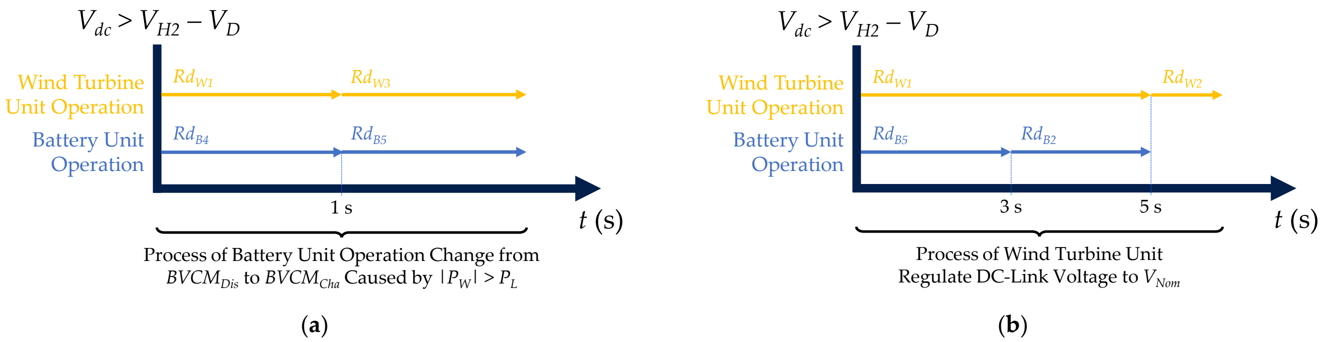

Figure 10. Transition operation of DC-link voltage and information transmission in case of $V_{dc} > V_{H2} - V_D$ because of the wind turbine unit WVDCM operation in islanded mode. (**a**) $V_{dc} > V_{H2} - V_D$ for process of battery unit operation change from $BVCM_{Dis}$ to $BVCM_{Cha}$ caused by $|P_W| > P_L$ in islanded mode; (**b**) $V_{dc} > V_{H2} - V_D$ for process of the wind turbine unit regulating the DC-link voltage to V_{Nom}.

4. Power Flow Control Strategy of Decentralized DCMG

In this section, the proposed PFCS is explained to realize an effective decentralized DCMG control and cooperation method with the EV unit. The PFCS determines the operating modes of all power units within the DCMG, by taking into account the factors such as wind power generation, load demand, battery SOC level, and availability of the utility grid unit. In addition, the grid-connected operation of the DCMG system also considers the electricity price condition to determine the suitable operation of the power units. The proposed PFCS is categorized into three main operation modes: grid-connected mode operation, islanded mode operation, and transition mode operation.

4.1. PFCS of Decentralized DCMG in Grid-Connected Mode

Table 2 shows the DCMG states and operation modes in the steady-state grid-connected mode. In this study, the DCMG states in the grid-connected mode are divided according to the electricity price conditions and battery SOC level as defined in Figure 2. As shown in Table 2, grid-connected operation modes at steady-state are determined according to the DCMG states. For example, DCMG state 1 represents the condition that the utility grid unit has the normal electricity price condition and the battery unit SOC level is in the F_B region. In DCMG state 1, the DCMG works with the operation mode OP_1.

Table 2. Steady-state DCMG states and operation modes in grid-connected mode (1 = True, 0 = False).

DCMG States	Conditions				Operation Modes
	High Electricity Price	Battery SOC			
		C_B	D_B or E_B	F_B	
1	0	0	0	1	OP_1
2	0	0	1	0	OP_2
3	0	1	0	0	OP_2
4	0	0	0	0	OP_2
5	1	0	0	1	OP_3
6	1	0	1	0	OP_3
7	1	1	0	0	OP_1

Table 3 shows the steady-state operation modes for individual power units in the grid-connected mode of the decentralized DCMG system.

Operation mode OP_1: In this mode, the utility grid unit operates with Rd_{G1} mode, the battery unit is in idle mode with Rd_{B3}, the wind turbine unit operates in the MPPT mode with Rd_{W3}, and all loads are connected. This operation mode is used in DCMG states 1 and 7. In either case, the battery enters idle mode to prevent further charging or discharging.

Table 3. Steady-state operation modes for individual power units of decentralized DCMG in grid-connected mode according to operation modes in Table 2.

Operation Modes	Operations of DCMG Units			
	Utility Grid Unit	Battery Unit	Wind Turbine Unit	Load Unit
OP_1	Rd_{G1}	Rd_{B3}	Rd_{W3}	R_T
OP_2	Rd_{G1}	Rd_{B2}	Rd_{W3}	R_T
OP_3	Rd_{G1}	Rd_{B1}	Rd_{W3}	R_T

Operation mode OP_2: In this mode, the utility grid unit operates with Rd_{G1} mode, the battery unit is in BCM mode with Rd_{B2}, the wind turbine unit operates in the MPPT mode with Rd_{W3}, and all loads are connected. This operation mode is used in DCMG state 2 through 4. In this case, the battery works in BCM mode to charge the battery to $SOC_{B,Max}$.

Operation mode OP_3: In this mode, the utility grid unit operates with Rd_{G1} mode, the battery unit is in BDM mode with Rd_{B1}, the wind turbine unit operates in the MPPT mode with Rd_{W3}, and all loads are connected. This operation mode is used in DCMG states 5 and 6. In this case, the battery works in BDM mode to supply power to DC-link.

4.2. PFCS of Decentralized DCMG in Islanded Mode

The proposed PFCS for the decentralized DCMG in the islanded mode are divided according to the load operation, the battery SOC level, and the wind turbine unit power condition. Tables 4–6 show the DCMG states and operation modes in the steady-state islanded mode, mainly according to the wind turbine power conditions. Table 4 denotes DCMG states and operations in the islanded mode for condition $|P_W| < P_L$. For example, the DCMG state 8 represents the condition that the load unit operates with total load R_T and the battery SOC level is in E_B or F_B region with $|P_W| < P_L$. In DCMG state 8, the DCMG works with the operation mode OP_4.

Table 4. Steady-state DCMG states and operation modes in islanded mode with condition $|P_W| < P_L$ (1 = True, 0 = False).

DCMG States	Conditions					Operation Modes
	Load	Battery SOC				
		B_B	C_B	D_B	E_B or F_B	
8	R_T	0	0	0	1	OP_4
9	R_T	0	0	1	0	OP_4
10	R_C	0	0	1	0	OP_5
11	R_C	0	1	0	0	OP_5
12	R_C	1	0	0	0	OP_5

Table 5 denotes DCMG states and operations in the islanded mode for condition $P_L + P_B > |P_W| > P_L$. In this Table, the DCMG state 13 represents the condition that the load unit operates with total load R_T and the battery SOC level is in the E_B region with $P_L + P_B > |P_W| > P_L$. In DCMG state 13, the DCMG works with the operation mode OP_6.

Table 6 denotes DCMG states and operations in the islanded mode for condition $|P_W| > P_L + P_B$. In this Table, DCMG state 20 represents the condition that the load unit operates with total load R_T and the battery SOC level is in the F_B region. In DCMG state 20, the DCMG works with the operation mode OP_9.

Table 7 shows the steady-state operation modes for individual power units in the islanded mode of the decentralized DCMG system.

Table 5. Steady-state DCMG states and operation modes in islanded mode with condition $P_L + P_B > |P_W| > P_L$ (1 = True, 0 = False).

DCMG States	Conditions						Operation Modes
	Load	Battery SOC					
		A_B	B_B	C_B	D_B	E_B	
13	R_T	0	0	0	0	1	OP_6
14	R_T	0	0	0	1	0	OP_6
15	R_C	0	0	0	1	0	OP_7
16	R_C	0	0	1	0	0	OP_7
17	R_C	0	1	0	0	0	OP_7
18	No load	0	1	0	0	0	OP_8
19	No load	1	0	0	0	0	OP_8

Table 6. Steady-state DCMG states and operation modes in islanded mode with condition $|P_W| > P_L + P_B$ (1 = True, 0 = False).

DCMG States	Conditions							Operation Modes
	Load	Battery SOC						
		A_B	B_B	C_B	D_B	E_B	F_B	
20	R_T	0	0	0	0	0	1	OP_9
21	R_T	0	0	0	0	1	0	OP_{10}
22	R_T	0	0	0	1	0	0	OP_{10}
23	R_C	0	0	0	1	0	0	OP_{11}
24	R_C	0	0	1	0	0	0	OP_{11}
25	R_C	0	1	0	0	0	0	OP_{11}
26	No load	0	1	0	0	0	0	OP_{12}
27	No load	1	0	0	0	0	0	OP_{12}

Table 7. Steady-state operation modes for individual power units of decentralized DCMG in islanded mode according to operating modes in Tables 4–6.

Operation Modes	Operations of DCMG Units			
	Utility Grid Unit	Battery Unit	Wind Turbine Unit	Load Unit
OP_4	-	Rd_{B4}	Rd_{W3}	R_T
OP_5	-	Rd_{B4}	Rd_{W3}	R_C
OP_6	-	Rd_{B5}	Rd_{W3}	R_T
OP_7	-	Rd_{B5}	Rd_{W3}	R_C
OP_8	-	Rd_{B5}	Rd_{W3}	No load
OP_9	-	Rd_{B3}	Rd_{W2}	R_T
OP_{10}	-	Rd_{B2}	Rd_{W2}	R_T
OP_{11}	-	Rd_{B2}	Rd_{W2}	R_C
OP_{12}	-	Rd_{B2}	Rd_{W2}	No load

Operation mode OP_4: In this mode, the battery unit is in $BVCM_{Dis}$ with Rd_{B4}, the wind turbine unit operates in the MPPT mode with Rd_{W3}, and all loads are connected. This operation mode is used in DCMG states 8 and 9. In either case, the battery SOC level is higher than $SOC_{B,Emg\text{-}H}$. The battery unit regulates DC-link voltage to V_{Nom} and the wind turbine unit operates in MPPT mode as $|P_W| < P_L$.

Operation mode OP_5: This mode is similar to operation mode OP_4 except for the load unit that only operates with R_C. This mode is used in DCMG states 10 through 12. In this case, the battery unit regulates DC-link voltage to V_{Nom} and the wind turbine unit operates in MPPT mode. This operation mode is used after the R_{NC} load shedding because the battery SOC level is lower than $SOC_{B,Emg\text{-}H}$ or it does not fulfill R_{NC} reconnection condition.

Operation mode OP_6: In this mode, the battery unit is in $BVCM_{Cha}$ with Rd_{B5}, the wind turbine unit operates in the MPPT mode with Rd_{W3}, and all loads are connected. This mode is used in DCMG states 13 and 14. In either case, the battery SOC level is higher than $SOC_{B,Emg\text{-}H}$ but lower than $SOC_{B,Max}$.

Operation mode OP_7: This mode is similar to OP_6 except for the load unit that only operates with R_C. This mode is used in DCMG states 15 through 17. In this case, the battery unit regulates DC-link voltage to V_{Nom} and the wind turbine unit operates in MPPT mode with condition $P_L + P_B > |P_W| > P_L$. This mode is used after the R_{NC} load shedding because the battery SOC level is lower than $SOC_{B,Emg\text{-}H}$ or it does not fulfill the R_{NC} reconnection condition.

Operation mode OP_8: This mode is similar to OP_6 except that the load is not connected. This mode is used in DCMG states 18 and 19. In this case, the battery unit regulates DC-link voltage to V_{Nom} and the wind turbine unit operates in MPPT mode as $P_L + P_B > |P_W| > P_L$ with $P_L = 0$. This mode is used after the R_{NC} and R_C load shedding caused by insufficient power as the battery SOC level reaches $SOC_{B,Min}$, or if the battery SOC level still does not reach $SOC_{B,Emg\text{-}L}$ for R_C reconnection.

Operation mode OP_9: In this mode, the battery unit is in idle mode with Rd_{B3}, the wind turbine unit operates in the WVCM mode with Rd_{W2}, and all loads are connected. This mode is only used in DCMG state 20. In this case, the battery SOC level is higher than $SOC_{B,Max}$. The wind turbine unit regulates DC-link voltage to V_{Nom} in charging mode as $|P_W| > P_L + P_B$ with $P_B = 0$.

Operation mode OP_{10}: In this mode, the battery unit is in BCM with Rd_{B5}, the wind turbine unit operates in the WVCM mode with Rd_{W2}, and all loads are connected. This mode is used in DCMG states 21 and 22. In either case, the battery SOC level is higher than $SOC_{B,Emg\text{-}H}$ and lower than $SOC_{B,Max}$.

Operation mode OP_{11}: This mode is similar to OP_{10} except for the load unit that only operates with R_C. This mode is used in DCMG states 23 through 25, in which the battery unit is in maximum power charging and the wind turbine unit operates in WVCM mode as $|P_W| > P_L + P_B$. This mode is used after the R_{NC} load shedding because the battery SOC level is lower than $SOC_{B,Emg\text{-}H}$, or it does not fulfill the R_{NC} reconnection condition.

Operation mode OP_{12}: This mode is similar to OP_{10} except that the load is not connected. This mode is used in DCMG states 26 and 27, in which the battery unit is in maximum power charging and the wind turbine unit operates in WVCM mode as $|P_W| > P_L + P_B$ with $P_L = 0$. This mode is used after the R_{NC} and R_C load shedding caused by insufficient power as the battery SOC level reaches $SOC_{B,Min,}$ and the battery SOC level still does not reach $SOC_{B,Emg\text{-}L}$ for R_C reconnection.

4.3. Transition Mode Operations of Decentralized DCMG

Table 8 shows transition conditions and operation modes for the proposed PFCS which are used for transmitting information to other power units in this study. Thirteen transition states of T_1 through T_{13} are defined as follows:

Conditions for mode T_1: This transition condition happens when the utility grid unit electricity price is changed from normal to high. When this condition occurs, the utility grid unit reduces the DC-link voltage V_{L1} as shown in Figure 9a. Then, the battery unit acknowledges this information in the predetermined time.

Conditions for mode T_2: This transition condition happens when the utility grid unit electricity price is changed from high to normal. When this condition occurs, the utility grid unit increases the DC-link voltage to V_{H1} as shown in Figure 8e. Then, the battery unit acknowledges this information by detecting the voltage level.

Table 8. Transition conditions and operation modes of decentralized DCMG.

Conditions								Operation Modes
Utility Grid Unit	**Electricity Price**	**Battery SOC**	**Mode of Battery Unit**	**Mode of Wind Turbine Unit**	P_W	**Load Unit**	V_{dc}	
Normal	Normal → High	$A_B - F_B$	Rd_{B1}, Rd_{B2}, or Rd_{B3}	Rd_{W3}	$[-P_W^{max}, 0]$	R_T	V_{L1}	T_1
Normal	High → Normal	$A_B - F_B$	Rd_{B1}, Rd_{B2}, or Rd_{B3}	Rd_{W3}	$[-P_W^{max}, 0]$	R_T	V_{H1}	T_2
Normal	High	$A_B, B_B \rightarrow C_B$	Rd_{B2}	Rd_{W3}	$[-P_W^{max}, 0]$	R_T	V_{Nom}	T_3
Fault → Normal	Normal	$A_B - F_B$	Rd_{B2}, Rd_{B3}, Rd_{B4}, or Rd_{B5}	$Rd_{W2} \rightarrow Rd_{W3}$	$[-P_W^{max}, 0]$	R_T, R_C, No load	V_{H1}	T_4
Fault → Normal	High	$A_B - F_B$	Rd_{B2}, Rd_{B3}, Rd_{B4}, or Rd_{B5}	$Rd_{W2} \rightarrow Rd_{W3}$	$[-P_W^{max}, 0]$	R_T, R_C, No load	V_{H1}	T_4
Fault	-	C_B	Rd_{B6}	Rd_{W3}	$\lvert P_W \rvert < P_L$	R_T	$V_{Nom} \rightarrow V_{L2}$	T_5
Fault	-	$B_B - C_B$	Rd_{B7}	Rd_{W2}, Rd_{W3}	$[-P_W^{max}, 0]$	$R_T \rightarrow R_C$	V_{L2}	T_6
Fault	-	A_B	Rd_{B5}	Rd_{W3}	$\lvert P_W \rvert < P_L$	R_C → No load	$< V_{L3}$	T_7
Fault	-	C_B	Rd_{B8}	Rd_{W2}, Rd_{W3}	$\lvert P_W \rvert > P_L$	No load → R_C	V_{H1}	T_8
Fault	-	$E_B - F_B$	Rd_{B8}	Rd_{W2}, Rd_{W3}	$\lvert P_W \rvert > P_L$	$R_C \rightarrow R_T$	V_{H1}	T_9
Fault	-	$A_B - F_B$	$Rd_{B4} \rightarrow Rd_{B5}$	Rd_{W1}	$\lvert P_W \rvert > P_L$	R_T, R_C, No load	$>V_{H2} - V_D$	T_{10}
Fault	-	$A_B - F_B$	$Rd_{B5} \rightarrow Rd_{B2}$	Rd_{W1}	$\lvert P_W \rvert > P_L + P_B$	R_T, R_C, No load	$>V_{H2} - V_D$	T_{11}
Fault	-	F_B	Rd_{B3}	Rd_{W1}	$\lvert P_W \rvert > P_L$	R_T, R_C, No load	$>V_{H2} - V_D$	T_{12}
Fault	-	$B_B - F_B$	Rd_{B2}, Rd_{B3}, $Rd_{B5} \rightarrow Rd_{B4}$	$Rd_{W2} \rightarrow Rd_{W3}$	$\lvert P_W \rvert < P_L + P_B$	R_T or R_C	$<V_{L2}$	T_{13}

Conditions for mode T_3: This transition condition happens when the utility grid unit electricity price is high and the battery SOC level is lower than $SOC_{B,Emg\text{-}L}$.

Conditions for mode T_4: This transition condition happens when the utility grid unit is reconnected after a fault. By observing the DC-link voltage value, the battery unit recognizes that the utility grid is reconnected with normal or high electricity prices as in Figure 8c,d. The wind turbine unit also recognizes the reconnection of the utility grid unit, and returns to the MPPT mode. The load unit reconnection is also initiated.

Conditions for mode T_5: This transition condition happens when the battery SOC level reaches $SOC_{B,Emg\text{-}H}$ in the islanded mode. The battery unit reduces the DC-link voltage to V_{L2} in discharging mode using $BVCM_{Emg1}$ for 0.5 s as shown in Figure 9d. This is to enable another ESS to regulate DC-link voltage to V_{Nom}.

Conditions for mode T_6: This transition condition happens after T_5 when the battery SOC level reaches $SOC_{B,Emg\text{-}H}$ in the islanded mode. The battery unit maintains the DC-link voltage at V_{L2} with Rd_{B7} during 5 s as shown in Figure 9d. The load unit then recognizes the DC-link voltage value and activates R_{NC} shedding.

Conditions for mode T_7: This transition condition happens when the battery SOC level reaches $SOC_{B,Min}$ in the islanded mode. The battery unit operation is switched to $BVCM_{Cha}$ and the load unit activates R_C shedding as shown in Figure 9f.

Conditions for mode T_8: This transition condition happens when the battery SOC level reaches $SOC_{B,Emg\text{-}L}$ in the islanded mode after previous decrease below $SOC_{B,Min}$. The battery unit increases the DC-link voltage to V_{H1} as in Figure 8a. The load unit continuously monitors the DC-link voltage level and reconnects R_C.

Conditions for mode T_9: This transition condition happens when the battery SOC level reaches $SOC_{B,LR}$ in the islanded mode after previous decrease below $SOC_{B,Emg\text{-}H}$. The battery unit increases the DC-link voltage to V_{H1} as in Figure 8b. The load unit continuously monitors the DC-link voltage level and reconnects R_{NC}.

Conditions for mode T_{10}: This transition condition happens when the wind turbine unit power is higher than the load requirement, and the battery unit is in $BVCM_{Dis}$. The wind turbine unit increases the DC-link voltage and operates in WVDCM as in Figure 10a. The battery unit changes operation from $BVCM_{Dis}$ to $BVCM_{Cha}$ after 1 s. The wind turbine unit operates back to the MPPT mode as the battery unit regulates DC-link voltage in $BVCM_{Cha}$.

Conditions for mode T_{11}: This transition condition happens when the wind turbine unit power is higher than the load requirement, and the battery unit charges power. The wind turbine unit increases the DC-link voltage and operates in WVDCM as in Figure 10b. The battery unit changes operation from $BVCM_{Cha}$ to BCM after 3 s. The wind turbine unit operates in WVCM and regulates DC-link voltage after 5 s.

Conditions for mode T_{12}: This transition condition happens when the wind turbine unit power is higher than the load requirement, and the battery unit is in idle mode after reaching $SOC_{B,Max}$. The wind turbine unit increases the DC-link voltage and operates in WVDCM. After 5 s, the wind turbine unit operates in WVCM and regulates DC-link voltage.

Conditions for mode T_{13}: This transition condition happens when the wind turbine unit power is decreased. The wind turbine unit changes operation to the MPPT mode as soon as the DC-link voltage falls below V_{L2}. When the DC-link voltage reduces to V_{L2}, the battery unit also changes operation from $BVCM_{Cha}$, BCM, or idle mode, to $BVCM_{Dis}$, and then regulates the DC-link voltage.

Table 9 shows the transition operation modes for individual power units of the decentralized DCMG system.

Operation mode T_1: In this mode, the utility grid unit operates with Rd_{G2} mode to reduce the DC-link voltage to V_{L1} as in Figure 9a, the battery unit operates either in BCM with Rd_{B2} or idle mode with Rd_{B3}, and the wind turbine unit operates in the MPPT mode with Rd_{W3}, and all loads are connected. The battery unit then changes operation to BDM with Rd_{B1}, BCM with Rd_{B2}, or idle mode with Rd_{B3} depending on the battery SOC level. If the battery unit operates in BDM, then the next mode is OP_3. If the battery unit changes operation to idle mode, then the next mode is OP_1. If the battery SOC level is in A_B or B_B region, then the battery unit operates in BCM to charge until $SOC_{B,Emg\text{-}H}$ and the next mode is T_3.

Table 9. Transition operation modes for individual power units of decentralized DCMG according to operating conditions in Table 8.

Operation Modes	Operation Modes				Next Operation Mode
	Utility Grid Unit	Battery Unit	Wind Turbine Unit	Load Unit	
T_1	Rd_{G2}	Rd_{B2}, or Rd_{B3}	Rd_{W3}	R_T	OP_1, OP_3, or T_3
T_2	Rd_{G3}	Rd_{B1}, Rd_{B2}, or Rd_{B3}	Rd_{W3}	R_T	OP_1 or OP_2
T_3	Rd_{G1}	Rd_{B2}	Rd_{W3}	R_T	OP_1
T_4	Rd_{G3}	Rd_{B2}, Rd_{B3}, Rd_{B4}, or Rd_{B5}	Rd_{W2}, Rd_{W3}	R_T	OP_1, OP_2, OP_3, or T_3
T_5	-	Rd_{B6}	Rd_{W3}	R_T	T_6
T_6	-	Rd_{B7}	Rd_{W2}, Rd_{W3}	R_T	OP_5, OP_7, or OP_{11}
T_7	-	Rd_{B4}	Rd_{W1}	R_C	OP_8, or OP_{12}
T_8	-	Rd_{B8}	Rd_{W2}, Rd_{W3}	No load	OP_5, OP_7, or OP_{11}
T_9	-	Rd_{B8}	Rd_{W2}, Rd_{W3}	R_C	OP_4, OP_6, or OP_{10}
T_{10}	-	Rd_{B4}	Rd_{W1}	R_T, R_C, No load	OP_6, OP_7, or OP_8
T_{11}	-	Rd_{B5}	Rd_{W1}	R_T, R_C, No load	OP_{10}, OP_{11}, or OP_{12}
T_{12}	-	Rd_{B3}	Rd_{W1}	R_T	OP_9
T_{13}	-	Rd_{B2}, Rd_{B3}, or Rd_{B5}	Rd_{W2}	R_T, R_C, No load	OP_4, OP_5, or T_{10}

Operation mode T_2: In this mode, the utility grid unit operates with Rd_{G3} mode to increase the DC-link voltage to V_{H1} as in Figure 8e, the battery unit operates in BDM with Rd_{B1}, BCM with Rd_{B2}, or idle mode with Rd_{B3}, the wind turbine unit operates in the MPPT mode with Rd_{W3}, and all loads are connected. The battery unit then changes operation to either BCM with Rd_{B2}, or idle mode with Rd_{B3} depending on the battery SOC level. If the battery unit operates in BCM, then the next mode is OP_2. If the battery unit changes operation to idle mode, then the next mode is OP_1.

Operation mode T_3: In this mode, the utility grid unit operates with Rd_{G1} and regulates the DC-link voltage to V_{Nom}, the battery unit operates in BCM with Rd_{B2}, the wind turbine unit operates in the MPPT mode with Rd_{W3}, and all loads are connected. This mode follows T_1 when the battery SOC level is lower than $SOC_{B,Emg\text{-}L}$.

Operation mode T_4: In this mode, the utility grid unit operates with Rd_{G3} to increase the DC-link voltage to V_{H1}, the battery unit is in BCM with Rd_{B2}, idle mode with Rd_{B3}, $BVCM_{Dis}$ with Rd_{B4}, or $BVCM_{Cha}$ with Rd_{B5}, the wind turbine unit operates either in the MPPT mode with Rd_{W3}, or WVCM mode with Rd_{W2}, and the load unit operates with R_T, R_C, or no load connection. As shown in Figure 8c,d, if the load shedding has been previously activated, the load reconnection process is initiated. The wind turbine unit recognizes the DC-link voltage and returns to the MPPT mode from WVCM. The battery unit recognizes electricity price, and changes operation to BDM with Rd_{B1}, BCM with Rd_{B2}, or idle mode with Rd_{B3} depending on the battery SOC level. If the battery unit operates in BDM, then the next mode is OP_3. If the battery unit changes operation to idle mode, then the next mode is OP_1. If the battery unit operates in BCM with the normal electricity price condition, then the next mode is OP_2. If the battery unit operates in BCM with high electricity price, then the next mode is T_3.

Operation mode T_5: In this mode, the battery unit operates in the $BVCM_{Emg1}$ with Rd_{B6} and regulates DC-link voltage to V_{L2}, the wind turbine unit operates in the MPPT mode with Rd_{W3}, and all loads are connected. The next mode is T_6 to maintain the DC-link voltage with the battery unit operating in Rd_{B7} as in Figure 9d.

Operation mode T_6: In this mode, the battery unit operates with Rd_{B7} to maintain the DC-link voltage to V_{L2}, the wind turbine unit operates in the MPPT mode with Rd_{W3}, and all loads are connected. The load unit continuously monitors the DC-link voltage level and starts R_{NC} shedding as in Figure 9d. The next mode is OP_{11} if the previous steady-state operation of the battery unit is in BCM with Rd_{B2}. If the previous steady-state operation of the battery unit is in $BVCM_{Cha}$ with Rd_{B5}, then the next mode is OP_7 to change from $BVCM_{Emg2,Cha}$ to $BVCM_{Cha}$, or OP_5 to change from $BVCM_{Emg2,Dis}$ to $BVCM_{Dis}$.

Operation mode T_7: In this mode, the battery unit is in $BVCM_{Cha}$ with Rd_{B5} as the battery SOC level falls below $SOC_{B,Min}$, the wind turbine unit operates in the MPPT mode with Rd_{W3}, and only the critical load is connected. When the wind power is not sufficient for the load, the voltage is reduced, and R_C shedding is triggered as in Figure 9f.

Operation mode T_8: In this mode, the battery unit regulates the DC-link voltage to V_{H1} either in $BVCM_{LR,Cha,}$ or $BVCM_{LR,Dis}$ with Rd_{B8} as the battery SOC level reaches $SOC_{B,Emg\text{-}L}$, the wind turbine unit operates either in the MPPT mode with Rd_{W3} or in the WVCM with Rd_{W2}, and the load is not connected. The load unit monitors the DC-link voltage to reconnect R_C as in Figure 8a. The next mode is OP_{11} if the previous steady-state operation of the battery unit is in BCM with Rd_{B2}. If the previous steady-state operation of the battery unit is in $BVCM_{Cha}$ with Rd_{B5}, the next mode is OP_7 to change from $BVCM_{LR,Cha}$ to $BVCM_{Cha}$, or OP_5 to change from $BVCM_{LR,Dis}$ to $BVCM_{Dis}$.

Operation mode T_9: In this mode, the battery unit regulates the DC-link voltage to V_{H1} either in $BVCM_{LR,Cha,}$ or in $BVCM_{LR,Dis}$ with Rd_{B8} as the battery SOC level reaches $SOC_{B,LR}$, the wind turbine unit operates either in the MPPT mode with Rd_{W3} or in the WVCM with Rd_{W2}, and only the R_C load is connected. The load unit monitors the DC-link voltage to reconnect R_{NC} as in Figure 8b. The next mode is OP_{10} if the previous operation of the battery unit is in BCM with Rd_{B2}. If the previous operation of the battery unit is in $BVCM_{Cha}$ with Rd_{B5}, the next mode is OP_6 to change from $BVCM_{LR,Cha}$ to $BVCM_{Cha}$, or OP_4 to change from $BVCM_{LR,Dis}$ to $BVCM_{Dis}$.

Operation mode T_{10}: In this mode, the battery unit is in $BVCM_{Dis}$ with Rd_{B4}, the wind turbine unit operates in WVDCM with Rd_{W1}, and the load unit operates with R_T, $R_{C,}$ or no load connection. The DC-link voltage is increased by the wind turbine unit. The battery unit operation is changed from $BVCM_{Dis}$ with Rd_{B4} to $BVCM_{Cha}$ with Rd_{B5} and the wind turbine unit operates back in the MPPT mode as in Figure 10a. If the total load is connected, the next mode is OP_6. If only the R_C load is connected, the next mode is OP_7. Finally, if there is no load connection before T_{10}, the next mode is OP_8.

Operation mode T_{11}: In this mode, the battery unit is in $BVCM_{Cha}$ with Rd_{B5}, the wind turbine unit operates in the WVDCM with Rd_{W1}, and the load unit operates with R_T, $R_{C,}$ or no load connection. The DC-link voltage is increased by the wind turbine unit, the battery unit operation is changed from $BVCM_{Cha}$ with Rd_{B5} to BCM with Rd_{B2}, and the wind turbine unit regulates the DC-link voltage to V_{Nom} in WVCM with Rd_{W2} as in Figure 10b. If the total load is connected, the next mode is OP_{10}. If only R_C load is connected, the next mode is OP_{11}. Lastly, if there is no load connection, the next mode is OP_{12}.

Operation mode T_{12}: In this mode, the battery unit is in idle mode with Rd_{B3}, the wind turbine unit operates in WVDCM with Rd_{W1}, and all the loads are connected. The DC-link voltage is increased by the wind turbine unit, and the wind turbine unit regulates the DC-link voltage to V_{Nom} in WVCM with Rd_{W2} as in Figure 10b with the battery unit still working in idle. The next mode is OP_9.

Operation mode T_{13}: In this mode, the battery unit is in BCM with Rd_{B2}, $BVCM_{Cha}$ with Rd_{B5}, or idle mode with Rd_{B3}, the wind turbine unit operates in WVCM with Rd_{W2}, and the load unit operates with R_T, $R_{C,}$ or no load connection. The DC-link voltage is decreased as the wind turbine unit power is insufficient to regulate the DC-link voltage to V_{Nom}. As soon as the DC-link voltage falls below V_{L2}, the wind turbine unit operates in the MPPT mode with Rd_{W3} and the battery unit regulates the DC-link voltage to V_{Nom} with $BVCM_{Dis}$ with Rd_{B4}. If all the loads are connected, the next mode is OP_4. If only the R_C load is connected, the next mode is OP_5. If the load is not connected, the next mode is

T_{10}, in which the DC-link voltage is increased, and the battery unit changes operation to $BVCM_{Cha}$ with Rd_{B5}.

4.4. Co-Operation with EV Unit

The integration of an EV unit as additional ESS is also studied to improve the scalability of the proposed decentralized DCMG system. Figure 11 shows the operation modes for the EV unit. The operation modes of the EV unit only work at steady-state and consist of three grid-connected modes and four islanded modes. For the EV unit, operation modes are simplified without considering load shedding or load reconnection as in the battery unit because the EV can be disconnected from the DCMG at any time.

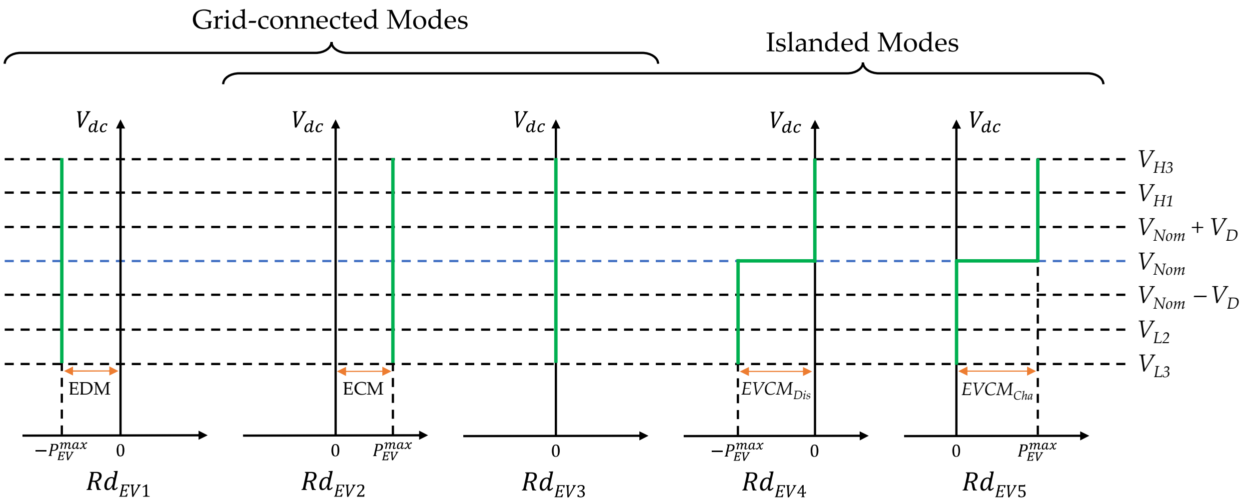

Figure 11. Operation modes of EV unit.

The first mode, Rd_{EV1}, is the EV maximum current discharging mode (EDM) that is used when the utility grid is in the high electricity price condition. The second mode, Rd_{EV2}, is the EV maximum current charging mode (ECM) that is used under the normal electricity price condition and the condition that the wind power unit regulates the DC-link voltage. The third mode, Rd_{EV3}, is the idle mode to stop charging when the EV SOC reaches $SOC_{EV,Max}$, or to stop discharging when the EV SOC reaches $SOC_{EV,Min}$, respectively. The fourth mode, Rd_{EV4}, is the EV voltage control mode by discharging ($EVCM_{Dis}$) that is used in the islanded mode when the battery unit cannot regulate the DC-link voltage because of the low battery SOC level. The fifth mode, Rd_{EV5}, is the EV voltage control by charging ($EVCM_{Cha}$) that is used to absorb excessive power from the DC-link. The $EVCM_{Dis}$ and $EVCM_{Cha}$ use the PI control to maintain the DC-link voltage at V_{Nom}.

Table 10 shows the EV SOC levels used in this study. Because the EV unit may connect and disconnect at any time, the transition modes for load shedding and load reconnection are not considered for the EV unit. The minimum and maximum SOC levels for the EV unit are used solely to prevent overdischarge and overcharge.

Table 10. SOC levels for EV unit.

SOC	Values	Purposes
$SOC_{EV,Min}$	30%	Level to stop discharging
$SOC_{EV,Max}$	90%	Level to stop charging

The EV unit also has the transition times to be able to cooperate with the battery unit. Figure 12 shows the transition operation of DC-link voltage and information transmission to cooperate with the EV unit. Figure 12a shows the battery and EV unit detection times for the utility grid unit fault when the previous utility grid unit operation is in the REC mode.

Even while the EV unit acknowledges the utility grid fault at the same instant as the battery unit, it operates in idle mode with Rd_{EV3}. The EV unit continuously monitors the DC-link voltage and regulates the DC-link voltage after 100 ms when the DC-link voltage is higher than $V_{H2} - V_D$. Figure 12b shows the process of utility grid fault identification by the EV unit when the previous utility grid unit operation is in INV mode. The entire process is similar to Figure 12a except that the EV unit takes the regulation of the DC-link voltage with Rd_{EV4} with the condition $V_{dc} < V_{L2}$. Figure 12c shows the EV detection process of insufficient power in the DCMG system. After 100 ms when the DC-link voltage is lower than or equal to V_{L2}, the EV unit regulates the DC-link voltage at V_{Nom} with Rd_{EV4}.

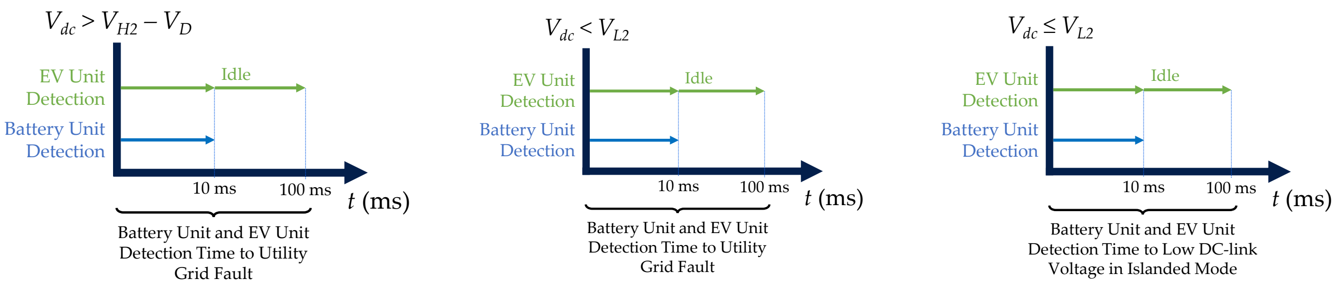

(**a**) (**b**) (**c**)

Figure 12. Transition operation of DC-link voltage and information transmission for the EV unit cooperation. (**a**) $V_{dc} > V_{H2} - V_D$ for process of utility grid fault; (**b**) $V_{dc} < V_{L2}$ for process of utility grid fault; (**c**) $V_{dc} \leq V_{L2}$ for process of insufficient power detection.

Figure 13 shows the transition operation of DC-link voltage and information transmission for the EV unit cooperation in the islanded mode in the case of $V_{dc} > V_{H2} - V_D$. Figure 13a shows the process of the EV unit operation change from idle to $EVCM_{Dis}$ and the battery unit operation change from $BVCM_{Cha}$ to BCM caused by $|P_W| > P_L + P_B$ in the islanded mode. This process occurs after the battery unit changes operations from $BVCM_{Dis}$ to $BVCM_{Cha}$ in Figure 10a. When $|P_W|$ is higher than P_L and P_B, the wind turbine unit operates in WVDCM and V_{dc} increases to the value of $V_{H2} - V_D$. By detecting this increased voltage, the EV unit operation is changed from Rd_{EV4} to Rd_{EV5} after 3 s. At the same time, the battery unit operation is changed from Rd_{B5} to Rd_{B2}. Then, the wind turbine unit operates back in the MPPT mode as the EV unit regulates DC-link voltage in $EVCM_{Cha}$.

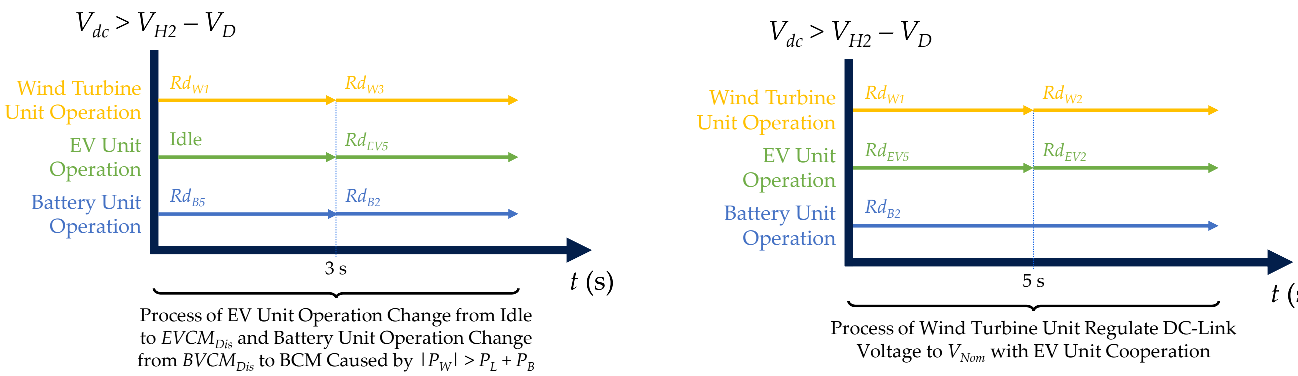

(**a**) (**b**)

Figure 13. Transition operation of DC-link voltage and information transmission for EV unit cooperation in case of $V_{dc} > V_{H2} - V_D$ because of the wind turbine unit WVDCM operation in islanded mode. (**a**) $V_{dc} > V_{H2} - V_D$ for process of EV unit operation change from idle to $BVCM_{Dis}$ and battery unit operation change from $BVCM_{Cha}$ to BCM caused by $|P_W| > P_L + P_B$ in islanded mode; (**b**) $V_{dc} > V_{H2} - V_D$ for process of the wind turbine unit regulating the DC-link voltage to V_{Nom}.

Figure 13b shows the process of the wind turbine unit regulating the DC-link voltage to V_{Nom}. When $|P_W|$ is higher than P_L even with the battery unit and the EV unit in charging operation, the wind turbine unit operates in WVDCM in Rd_{W1} and V_{dc} increases to the value of $V_{H2} - V_D$. Then, after 5 s, the EV unit changes the operation from $EVCM_{Cha}$ in Rd_{EV5} to ECM in Rd_{EV2}. After 5 s, the wind turbine unit changes operation from WVDCM in Rd_{W1} to WVCM in Rd_{W2}.

5. Simulation Results

In this section, the simulations for a decentralized DCMG are conducted by using the PSIM software to assess the feasibility and reliability of the proposed control scheme. To validate the effectiveness under various uncertain DCMG operations, the simulation tests consider several scenarios such as electricity price changes, transition from the grid-connected mode to islanded mode, emergency SOC in the islanded mode, load reconnection in the islanded mode, voltage regulation by the wind turbine in the islanded mode, and the involvement of EV units. Detailed system parameters can be found in Table 11. Throughout the simulation results, P_G, P_W, P_B, and P_L stand for the power of the utility grid unit, wind turbine unit, battery unit, and load unit, respectively. It is worth mentioning that the power flow direction follows the definition in Section 2.

Table 11. System parameters of a decentralized DCMG system.

Power Units	Parameters	Symbol	Value
Utility grid unit	Grid voltage	V_G^{rms}	220 V
	Grid frequency	f_G	60 Hz
	Transformer Y/Δ	T	380/220 V
	Inverter-side inductance of LCL filter	L_1	1.7 mH
	Parasitic resistance in L_1	R_1	0.5 Ω
	Grid-side inductance of LCL filter	L_2	1.7 mH
	Parasitic resistance in L_2	R_2	0.5 Ω
	Filter capacitance of LCL filter	C_f	4.5 μF
Wind turbine unit	PMSG stator resistance	R_S	0.64 Ω
	PMSG *dq*-axis inductance	L_{dq}	0.82 mH
	PMSG number of poles	p	6
	PMSG inertia	J	0.111 kgm^2
	PMSG flux linkage	ψ	0.18 Wb
	Converter filter inductance	L_W	7 mH
	Maximum power of the wind turbine unit	P_W^{max}	−1500 W
Battery unit	Rated capacity	C	25 Ah
	Maximum power	P_B^{max}	450W
	Maximum voltage	V_B^{max}	180 V
	Initial no-load voltage	V_{NL_0}	400 V
	Droop constant	R_d	0.0111
	Converter filter inductance L	L_B	7 mH
Load unit	Power of non-critical load	P_{NC}	200 W
	Power of critical load	P_C	200 W
DC-link	Nominal DC-link voltage	V_{Nom}	400 V
	First level of low DC-link voltage	V_{L1}	385 V
	Second level of low DC-link voltage	V_{L2}	370 V
	Third level of low DC-link voltage	V_{L3}	360 V
	First level of high DC-link voltage	V_{H1}	415 V
	Second level of high DC-link voltage	V_{H2}	430 V
	Third level of high DC-link voltage	V_{H3}	440 V
	Droop voltage constant	V_D	5 V
	Capacitance	C_{dc}	4 mF

5.1. Case of Electricity Price Changes

Figure 14 shows the simulation result for the grid-connected case with the transition of the electricity price from normal to high as well as the wind power increase at t = 5 s and decrease at t = 7 s. Initially, the DCMG system starts at t = 1 s with OP_2 in the grid-connected mode. The DC-link voltage V_{dc} is regulated to V_{Nom} by the utility grid unit. The battery unit is in BCM mode, and the wind turbine unit is in the MPPT mode. When the electricity price is changed to high at t = 3 s, the utility grid unit regulates V_{dc} to V_{L1} for 5 s until t = 8 s in mode T_1. In 3 s after V_{dc} is reduced, the battery unit recognizes the high electricity price condition and changes operation to BDM. As explained in Figure 9a, the transition process is completed at t = 8 s and the DCMG system operates in OP_3 at steady-state with V_{dc} returning to V_{Nom}. In mode OP_3, the battery is in maximum power discharging to minimize the electricity cost by maximizing the power injection into the utility grid if SOC_B is higher than $SOC_{B,Emg\text{-}H}$.

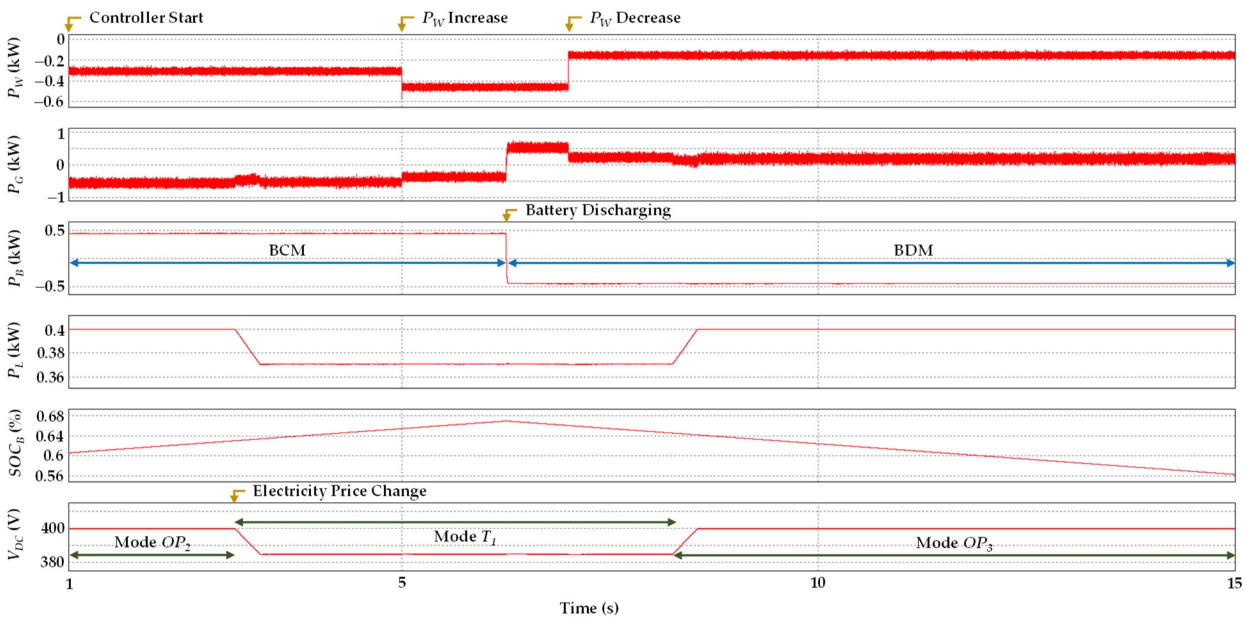

Figure 14. Simulation result in case of electricity price change from normal to high.

5.2. Case of Grid-Connected Mode to Islanded Mode

Figure 15 shows the simulation result for the transition from the grid-connected mode to islanded mode. Initially, the DCMG system is in mode OP_1 at t = 3 s. In this mode, the wind turbine unit operates in the MPPT mode, the battery unit is in idle mode with Rd_{B3} as the battery SOC level is higher than $SOC_{B,Max}$, the utility grid unit regulates V_{dc} to V_{Nom} with Rd_{G1}, and all the loads are connected. As the utility grid unit fault occurs at t = 4 s, V_{dc} decreases. The battery unit monitors V_{dc} and changes operation to $BVCM_{Dis}$ with Rd_{B4} when V_{dc} drops below V_{L2} after 10 ms as shown in Figure 9c. As a result, the operation mode is changed to OP_4, in which the battery unit regulates V_{dc} to V_{Nom} in the islanded mode, the wind turbine unit operates in the MPPT mode, and all the loads are connected.

5.3. Case of Emergency SOC in Islanded Mode

To verify the reliability of the proposed battery SOC management feature, the simulation result in case of emergency SOC level in the islanded mode is presented in Figure 16. The DCMG system initially operates in OP_4 at t = 1 s. The wind turbine unit operates in the MPPT mode, the battery unit regulates V_{dc} to V_{Nom} in $BVCM_{Dis}$ with Rd_{B4} in the islanded mode, and all the loads are connected. The battery SOC level slowly decreases because of discharging operation. As soon as the battery SOC level reaches $SOC_{B,Emg\text{-}H}$ in the islanded mode, the DCMG operation is changed to mode T_5, in which the battery unit works as

$BVCM_{Emg1}$ to reduce V_{dc} to V_{L2} during 0.5 s. After that, the DCMG operation is changed again to T_6, in which the battery unit maintains V_{dc} at V_{L2} with $BVCM_{Emg2,Dis}$. The load unit continues to monitor V_{dc}, and triggers R_{NC} shedding after 3 s when V_{dc} is reduced as shown in Figure 9d. Then, after 5 s when V_{dc} is reduced, the DCMG works as steady-state mode OP_5, in which the battery unit regulates V_{dc} at V_{Nom} using $BVCM_{Dis}$ with Rd_{B4}, the wind turbine unit operates in the MPPT mode, and the load unit only operates with R_C.

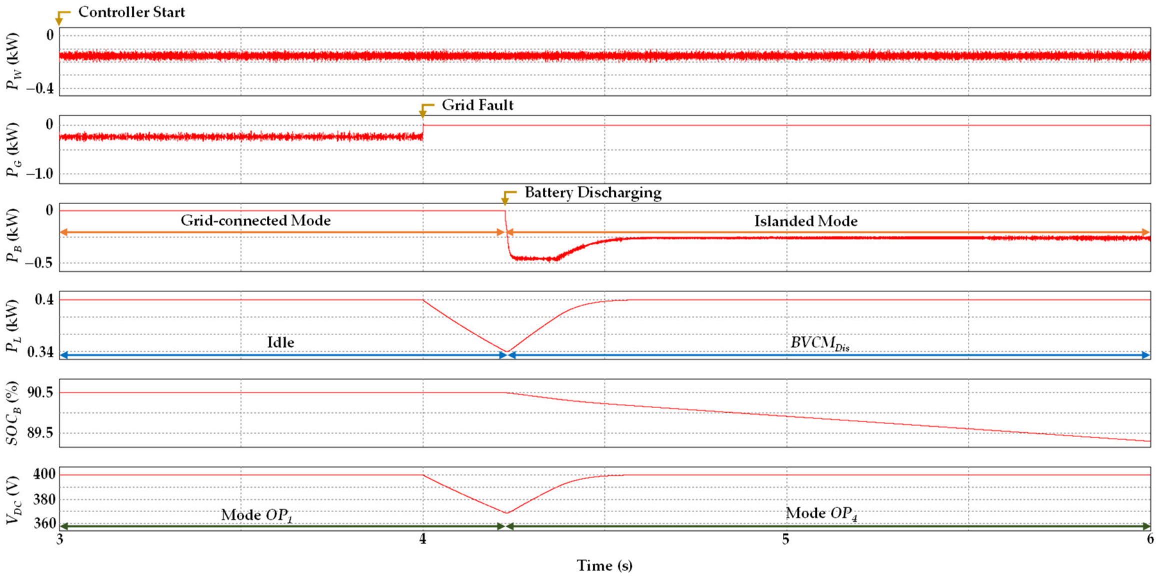

Figure 15. Simulation result for the transition from grid-connected mode to islanded mode.

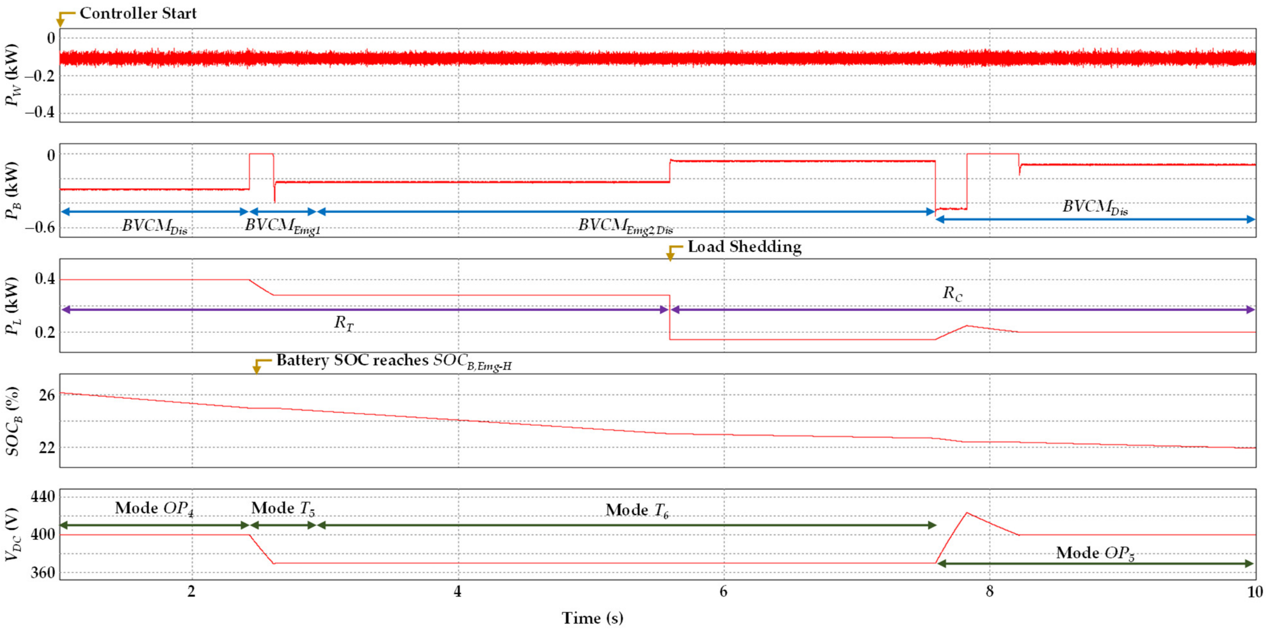

Figure 16. Simulation result in case of emergency SOC in islanded mode.

5.4. Case of Load Reconnection in Islanded Mode

Figure 17 presents the simulation result for the proposed PFCS in case of load reconnection in the islanded mode. First, the DCMG system operates with OP_7 at t = 1 s. In this mode, the wind turbine unit operates in the MPPT mode, the battery unit regulates V_{dc} with $BVCM_{Cha}$ with Rd_{B5}, and the load unit only operates with R_C. The battery SOC level increases when operated with $BVCM_{Cha}$. As soon as the battery SOC level reaches $SOC_{B,LR}$ around t = 4 s, the battery unit changes operation to T_9. In this mode, the battery unit operates in $BVCM_{LR,Dis}$ to increase V_{dc} immediately to V_{H1} and then changes operation to $BVCM_{LR,Cha}$ to maintain V_{dc} at V_{H1}. The load unit monitors V_{dc}, and reconnects the R_C load after 8 s (around t = 12 s). After load reconnection, the battery unit operation is changed to $BVCM_{LR,Dis}$ to maintain V_{dc} to V_{H1}. After the transition for load reconnection is finished, the DCMG operates in steady-state mode OP_4 around t = 14 s, in which the wind turbine unit operates in the MPPT mode, the battery unit is in $BVCM_{Dis}$ with Rd_{B4}, and all the loads are connected.

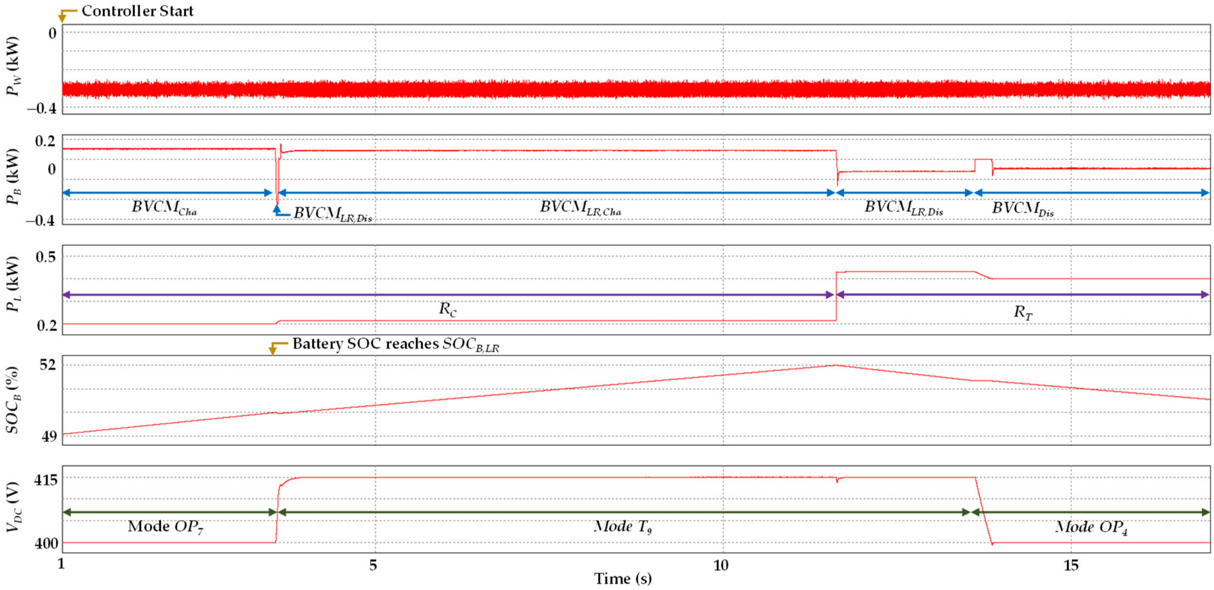

Figure 17. Simulation result in case of load reconnection in islanded mode.

5.5. Case of Voltage Regulation by Wind Turbine Unit in Islanded Mode

Figure 18 shows the simulation result for the proposed PFCS in case of voltage regulation by the wind turbine unit in the islanded mode. Initially, the DCMG system operates with OP_6 at t = 1 s, in which the wind turbine unit operates in the MPPT mode, the battery unit regulates V_{dc} with $BVCM_{Cha}$ with Rd_{B5}, and all the loads are connected in the load unit. As soon as the battery SOC level reaches $SOC_{B,Max}$ around t = 4 s, the battery unit changes operation to idle mode with Rd_{B3}. Because this produces a V_{dc} rise, the DCMG operation is changed to mode T_{12}, in which the wind turbine unit operates in WVDCM with Rd_{W1}. The wind turbine unit monitors V_{dc} and changes the operation mode after 5 s (around t = 9 s) to WVCM with Rd_{W2}, which results in the DCMG operation change to OP_9. In this operation, the wind turbine unit regulates V_{dc}, the battery unit is in idle mode, and all the loads are connected.

5.6. Case of EV Unit Involvement

To demonstrate the scalability of the proposed PFCS for the decentralized DCMG system, Figure 19 shows the simulation result in the case of the EV unit connection when the battery SOC level reaches $SOC_{B,Emg\text{-}H}$ in the islanded mode. Initially, the wind turbine unit is in the MPPT mode, the battery unit regulates V_{dc} in $BVCM_{Dis}$ with Rd_{B4}, and the EV unit is in idle mode with Rd_{EV3}. As the battery SOC level reaches $SOC_{B,Emg\text{-}H}$ around t = 2.5 s, the battery unit changes operation to $BVCM_{Emg1}$ with Rd_{B6} and decreases V_{dc} to V_{L2}. The EV unit monitors V_{dc}, and changes operation to $EVCM_{Dis}$ with Rd_{EV4} after 100 ms to regulate V_{dc} back to V_{Nom}. The battery unit remains idle when the EV undertakes the regulation of V_{dc} to V_{Nom}.

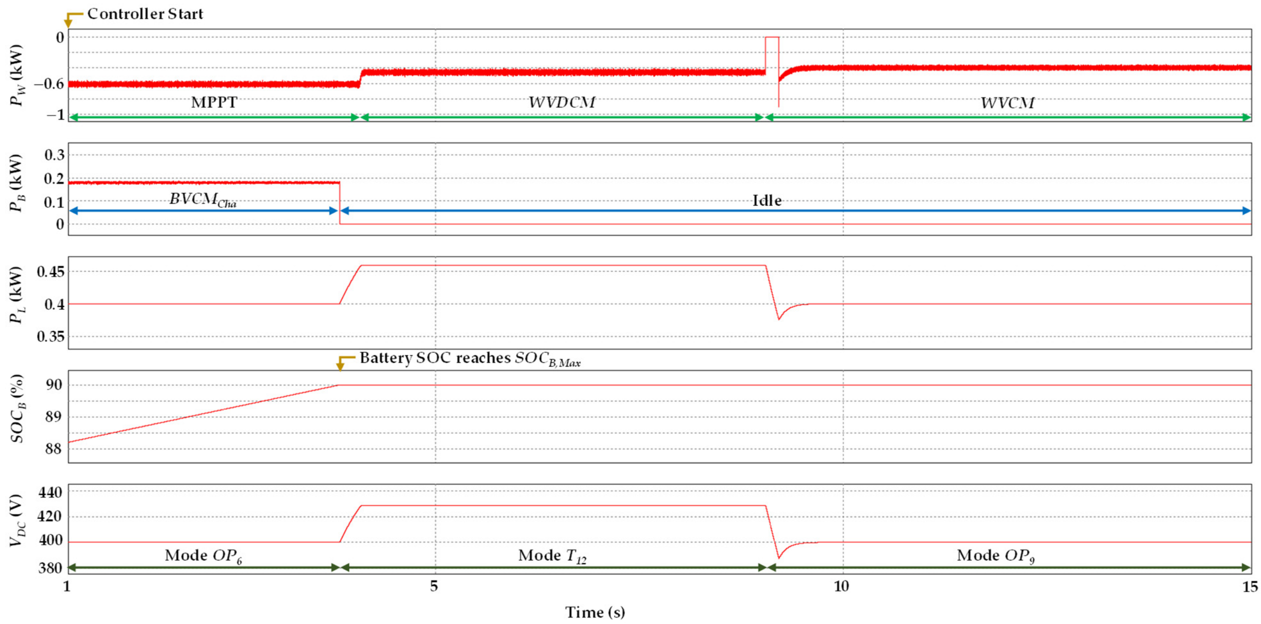

Figure 18. Simulation result in case of voltage regulation by wind turbine unit in islanded mode.

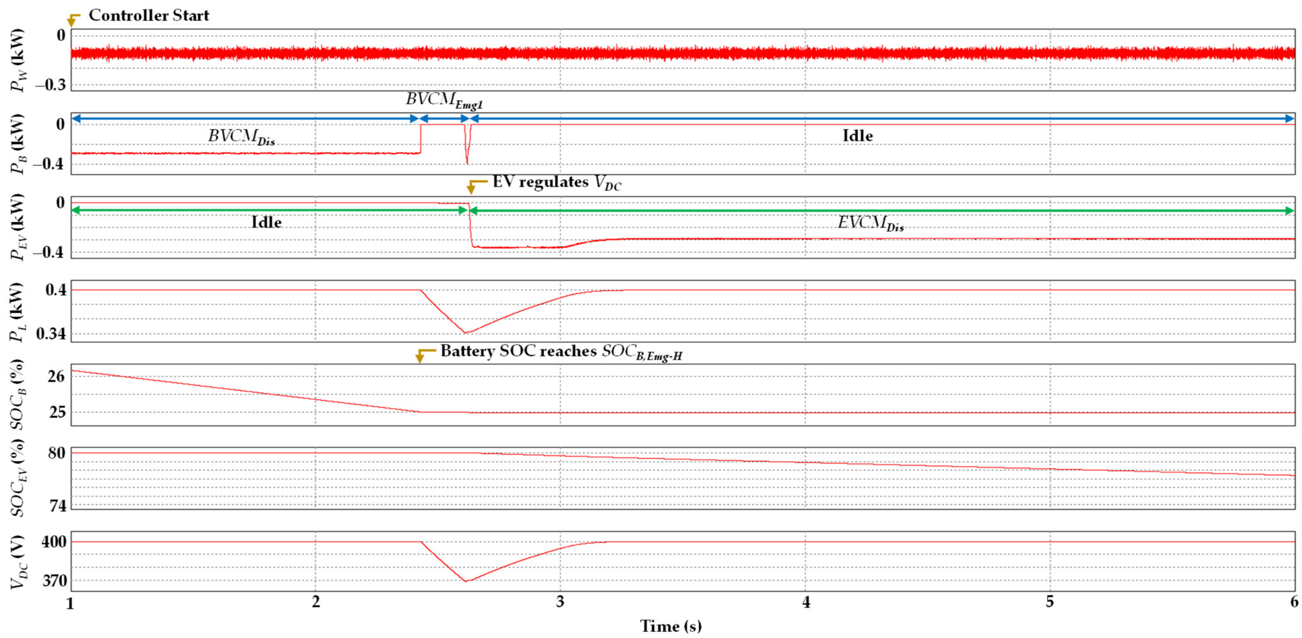

Figure 19. Simulation result in case of EV unit connection when battery SOC level reaches $SOC_{B,Emg\text{-}H}$ in islanded mode.

6. Experimental Results

The decentralized DCMG experimental setup, depicted in Figure 20, is used to demonstrate the feasibility of the proposed PFCS with the system parameters in Table 11. The experiment was performed with a laboratory-scale prototype DCMG system which has a similar power rating to the studies in [12–14]. The experimental DCMG system comprises four power electronic converters, which interface the DC-link with the utility grid unit, battery unit, wind turbine unit, and EV unit. The utility grid unit is connected to a three-phase main grid via a Y-Δ transformer and bidirectional AC/DC converter equipped with an LCL filter. The wind turbine unit combines a PMSG with an induction machine to transmit power to the DC-link through a unidirectional AC/DC converter. The battery and EV units utilize bidirectional interleaved DC/DC converters to connect a bidirectional

DC power source, serving as a battery. The magnetic contactors are used in the load unit. Power converters are implemented using a digital signal processor (DSP) TMS320F28335. The experimental tests are performed considering six scenarios: electricity price change, transition from the grid-connected to islanded mode, emergency SOC operation in the islanded mode, load reconnection in the islanded mode, voltage regulation by the wind turbine unit, and involvement of the EV unit.

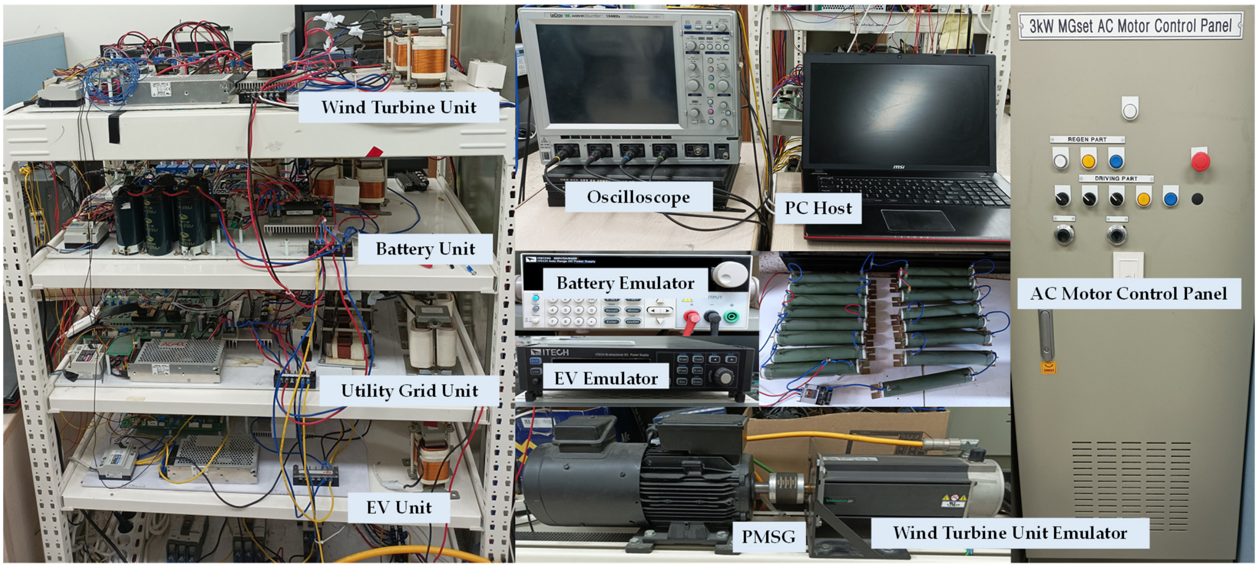

Figure 20. Configuration of experimental decentralized DCMG test setup.

6.1. Case of Electricity Price Changes

Figure 21 shows the experimental result of the proposed PFCS for a decentralized DCMG system when the grid electricity price changes from normal to high. The DCMG system initially works in OP_2, in which the wind turbine unit operates in the MPPT mode, the battery unit is in BCM mode with Rd_{B2}, and the utility grid unit regulates V_{dc} to V_{Nom} with Rd_{G1}. When the electricity price is changed to high, the operation is changed to T_1. In this mode, the utility grid unit operates with Rd_{B2} and regulates V_{dc} to V_{L1}. The battery unit monitors V_{dc}, and changes operation to BDM with Rd_{B1} in 3 s after the instant that the V_{dc} reduces to V_{L1}. After 5 s from the instant the V_{dc} reduces to V_{L1}, the DCMG operation is returned to OP_3, in which the utility grid unit regulates V_{dc} back to V_{Nom}, the battery unit is in BDM mode with Rd_{B1}, and the wind turbine unit operates in the MPPT mode.

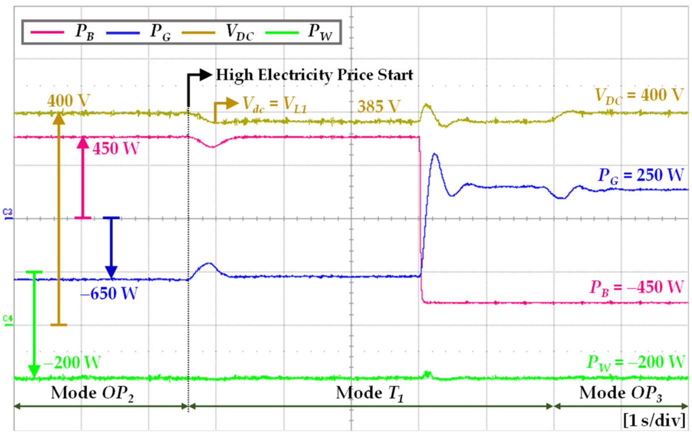

Figure 21. Experimental result of the proposed PFCS in grid-connected mode when grid electricity price is changed from normal to high.

Figure 22 shows the experimental result of the proposed PFCS when the grid electricity price changes from high to normal. The DCMG system initially runs in OP_3, in which the wind turbine unit operates in the MPPT mode, the battery is in BDM mode with Rd_{B1}, and the grid regulates V_{dc} to V_{Nom} with Rd_{G1}. When the electricity price is changed to normal, the operation is changed to T_2. In this mode, the utility grid unit operates with Rd_{B3} and regulates V_{dc} to V_{H1}. The battery unit monitors V_{dc}, and changes operation to BCM with Rd_{B2} in 18 s after that V_{dc} increased to V_{H1}. In the 20 s after V_{dc} increased to V_{H1}, the DCMG operation is returned to OP_2, in which the utility grid unit regulates V_{dc} back to V_{Nom}, the battery unit is in BCM mode with Rd_{B2}, and the wind turbine unit operates in the MPPT mode.

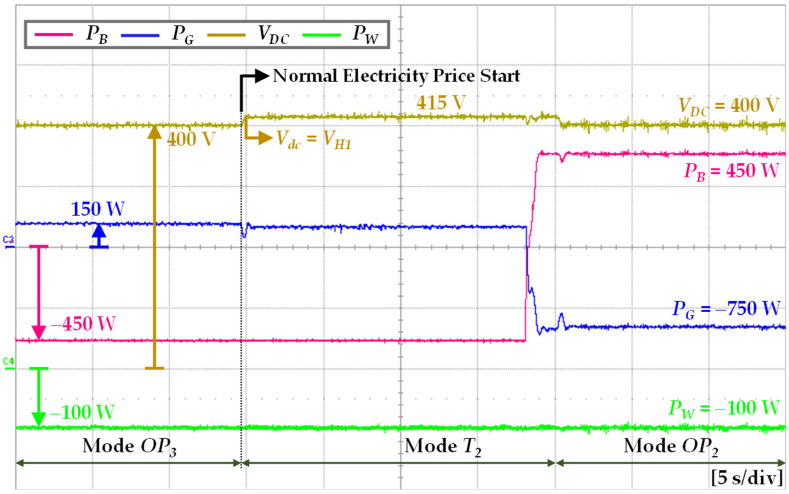

Figure 22. Experimental result of the proposed PFCS in grid-connected mode when grid electricity price is changed from high to normal.

6.2. Case of Transition from Grid-Connected Mode to Islanded Mode

Figure 23 shows the experimental result of the proposed PFCS under the transition from the grid-connected mode to islanded mode. Initially, the DCMG system is in OP_2, in which the wind turbine unit operates in the MPPT mode, the battery unit is in BCM mode with Rd_{B2}, the utility grid unit regulates V_{dc} to V_{Nom} with Rd_{G1}, and all the loads are connected. When the utility grid is disconnected due to a fault, the V_{dc} starts to decrease. The battery unit continuously monitors V_{dc} and changes operation to $BVCM_{Dis}$ with Rd_{B4} in the 10 ms after V_{dc} falls to V_{L2}. As a result, the DCMG operation is changed to OP_4, in which the battery regulates V_{dc} to V_{Nom} in the islanded mode, the wind operates in the MPPT mode, and all the loads are connected.

6.3. Case of Emergency SOC in Islanded Mode

To verify the battery SOC management feature of the proposed PFCS, Figure 24 presents the experimental result when the battery SOC reaches $SOC_{B,Emg\text{-}H}$ in the islanded mode. The DCMG system initially operates in OP_4, in which the wind turbine unit operates in the MPPT mode, the battery unit regulates V_{dc} to V_{Nom} using $BVCM_{Dis}$ with Rd_{B4}, and all the loads are connected. As soon as the battery SOC level reaches $SOC_{B,Emg\text{-}H}$ in the islanded mode, the DCMG operation is changed to T_5 as the battery unit changes operation to $BVCM_{Emg1}$ to reduce V_{dc} to V_{L2} during 0.5 s. After that, the DCMG operation is changed again to T_6, in which the battery unit maintains V_{dc} at V_{L2}. The load unit monitors V_{dc} and triggers R_{NC} shedding in 3 s after that V_{dc} is reduced. In 5 s after that V_{dc} is reduced to V_{L2}, the DCMG operation is changed to OP_5, in which the battery unit regulates V_{dc} at V_{Nom} using $BVCM_{Dis}$ with Rd_{B4}, the wind turbine unit operates in the MPPT mode, and only R_C is connected in the load unit.

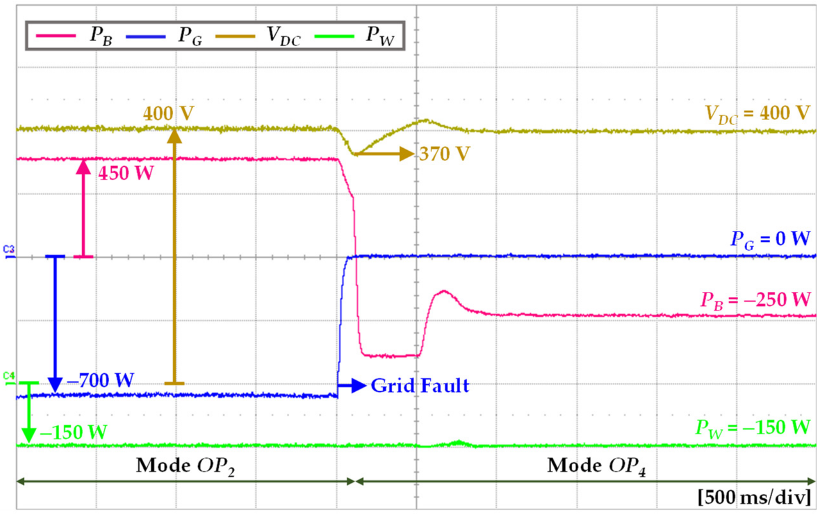

Figure 23. Experimental result of the proposed PFCS in case of the transition from grid-connected mode to islanded mode.

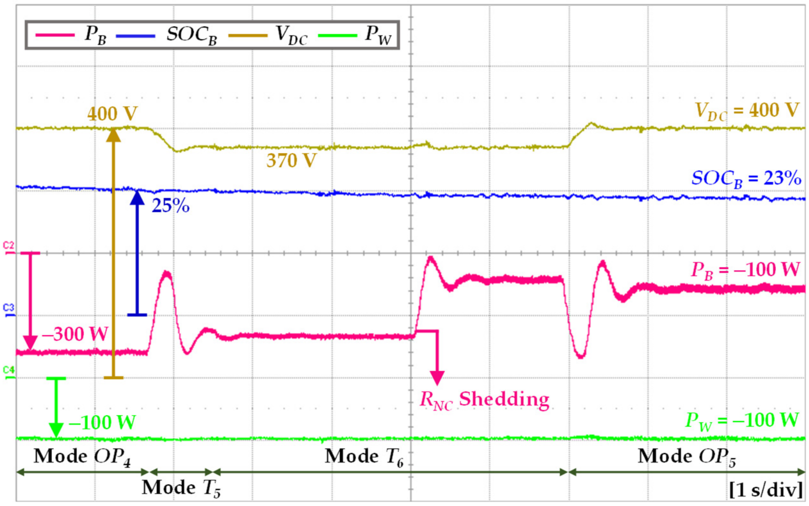

Figure 24. Experimental result of the proposed PFCS when the battery SOC level reaches emergency case, $SOC_{B,Emg\text{-}H}$ in islanded mode.

6.4. Case of Load Reconnection in Islanded Mode

Figure 25 shows the experimental result of the proposed PFCS when the battery SOC level reaches load reconnection level, $SOC_{B,LR}$ in the islanded mode. First, the DCMG system operates in OP_7, in which the wind turbine unit operates in the MPPT mode, the battery unit regulates V_{dc} with $BVCM_{Cha}$ with Rd_{B5}, and the load unit only operates with R_C. The battery SOC level increases with $BVCM_{Cha}$ operation. As soon as the battery SOC level reaches $SOC_{B,LR}$, the battery unit changes operation to $BVCM_{LR,Cha}$ with Rd_{B8} and the DCMG starts to operate in T_9 in which the battery unit increases V_{dc} to V_{H1}. The load unit monitors V_{dc} and then reconnects R_C load after 8 s. After load reconnection, the DCMG operates in steady-state OP_4, in which the battery operates in $BVCM_{Dis}$ with Rd_{B4}, the wind turbine unit operates in the MPPT mode, and all loads are connected.

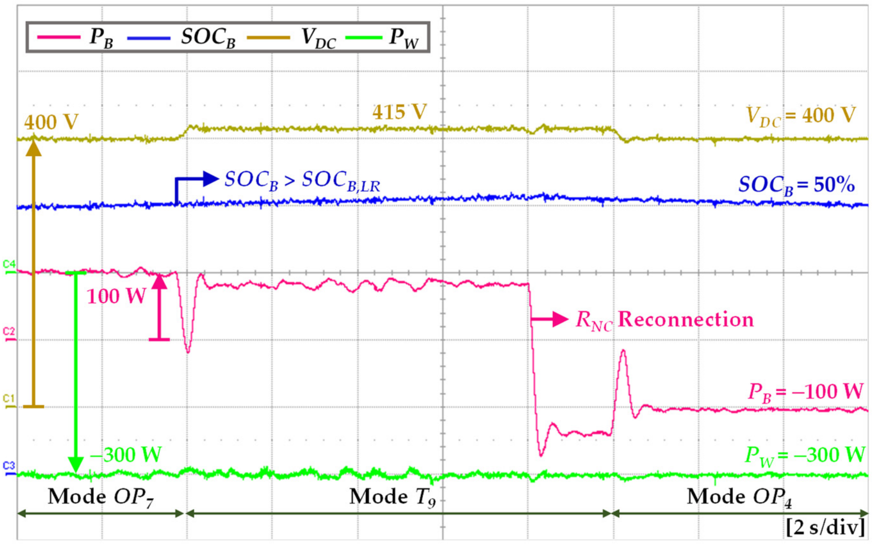

Figure 25. Experimental result of the proposed PFCS when the battery SOC level reaches load reconnection level ($SOC_{B,LR}$) in islanded mode.

6.5. Case of Voltage Regulation by Wind Turbine Unit in Islanded Mode

Figure 26 shows the experimental result of the proposed PFCS when the wind turbine unit regulates V_{dc} in the islanded mode. Initially, the DCMG system operates in OP_6, in which the wind turbine unit operates in the MPPT mode, the battery unit regulates V_{dc} in $BVCM_{Cha}$ with Rd_{B5}, and all loads are connected in the load unit. As soon as the battery SOC level reaches $SOC_{B,Max}$, the battery unit operation is changed to idle mode with Rd_{B3}. Because it results in the wind turbine power being higher than the load requirements, V_{dc} increases, and the wind turbine unit operates in WVDCM with Rd_{W1}. Then, the DCMG operation is changed to T_{12}. As shown in Figure 10b, 5 s after the instant of V_{dc} increase, the wind turbine unit changes the operation to WVCM with Rd_{W2}, which changes the DCMG operation to OP_9. In this mode, the wind turbine unit regulates V_{dc}, the battery unit is in idle mode, and all loads are connected.

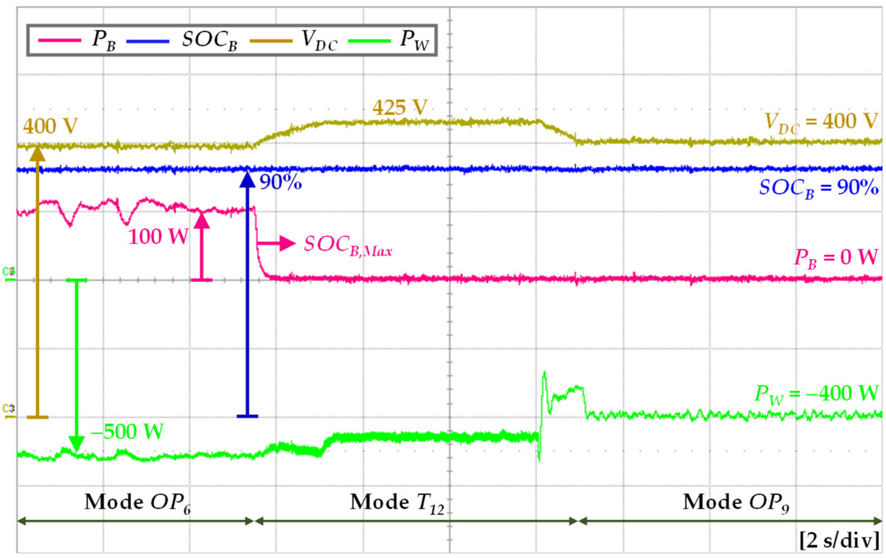

Figure 26. Experimental result of the proposed PFCS in case of voltage regulation by wind turbine unit in islanded mode.

6.6. Case of EV Unit Involvement

To demonstrate the scalability of the proposed PFCS of the decentralized DCMG system, Figure 27 shows the experimental result in case of the EV unit connection specifically when the battery SOC level reaches $SOC_{B,Emg\text{-}H}$ in the islanded mode. Initially, the wind turbine unit is in the MPPT mode, the battery unit regulates V_{dc} in $BVCM_{Dis}$ with Rd_{B4}, and the EV unit is in idle mode with Rd_{EV3}. When the battery SOC level reaches $SOC_{B,Emg\text{-}H}$, the battery unit operation is changed to $BVCM_{Emg1}$ with Rd_{B6} and V_{dc} is decreased to V_{L2}. By monitoring V_{dc} level, the EV unit changes operation to $EVCM_{Dis}$ with Rd_{EV4} 100 ms after the instant that V_{dc} is decreased to V_{L2}, as shown in Figure 12c. The V_{dc} is then gradually increased to V_{Nom} as the EV unit injects the maximum power. It is confirmed from this result that the proposed PFCS exhibits the scalable feature because the EV unit can operate as additional ESS to support the battery when the battery SOC level approaches a low level.

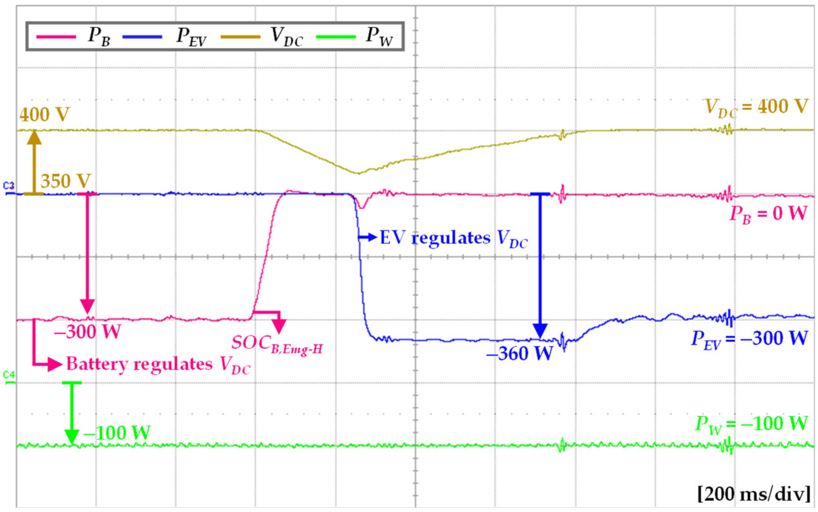

Figure 27. Experimental result of the proposed PFCS in case of EV unit involvement.

7. Conclusions

With the aim of enhancing the reliability and optimizing the DCMG operation, this paper has presented a PFCS for a decentralized DCMG system. The proposed PFCS utilizes the transition mode operations to transmit the information on the DCMG system to other power units without using additional DCLs. During the transition operation modes, the transmitting power unit adjusts the DC-link voltage level, while the receiving power unit continuously monitors the DC-link voltage with the predetermined intervals. If uncertain conditions arise in a specific power unit, this power unit activates the transition operation mode to propagate this information to all power units in the DCMG system. After this uncertain condition is acknowledged by all power units, the DCMG operation is switched back from the transition operation mode to the optimal steady-state operation. The proposed PFCS greatly improves the flexibility of the decentralized DCMG system even under various factors such as electricity price change, grid availability, battery SOC level, and wind power variation. The DC-link voltage can be effectively maintained at the nominal value at steady-state conditions by the proposed PFCS regardless of the grid-connected or islanded mode. The DCMG system reliability is also improved by incorporating the battery SOC management strategy. Furthermore, the scalability issue of the DCMG system is also studied by considering an EV unit as an additional ESS in the DCMG system. Simulation and experimental results under various conditions have been presented to verify the performance of the proposed PFCS. The results clearly confirm the reliability and flexibility of the proposed PFCS.

Author Contributions: M.A.M.J., D.T.T. and K.-H.K. conceived the main concept of the DC microgrid control structure and developed the entire system. M.A.M.J. and D.T.T. carried out the research and analyzed the numerical data with guidance from K.-H.K.; M.A.M.J., D.T.T. and K.-H.K. collaborated in the preparation of the manuscript. All authors have read and agreed to the published version of the manuscript.

Funding: This research was supported by Basic Science Research Program through the National Research Foundation of Korea (NRF) funded by the Ministry of Education (NRF-2019R1A6A1A03032119). This work was supported by the National Research Foundation of Korea (NRF) grant funded by the Korea government (MSIT) (NRF-2022R1F1A1064350).

Institutional Review Board Statement: Not applicable.

Informed Consent Statement: Not applicable.

Data Availability Statement: Data sharing is not applicable to this article.

Conflicts of Interest: The authors declare no conflict of interest.

References

1. Carpintero-Rentería, M.; Santos-Martín, D.; Guerrero, J.M. Microgrids literature review through a layers structure. *Energies* **2019**, *12*, 4381. [CrossRef]
2. Ansari, S.; Chandel, A.; Tariq, M. A comprehensive review on power converters control and control strategies of AC/DC microgrid. *IEEE Access* **2020**, *9*, 17998–18015. [CrossRef]
3. Al-Ismail, F.S. DC microgrid planning, operation, and control: A comprehensive review. *IEEE Access* **2021**, *9*, 36154–36172. [CrossRef]
4. Ensermu, G.; Bhattacharya, A.; Panigrahy, N. Real-time simulation of smart DC microgrid with decentralized control system under source disturbances. *Arab. J. Sci. Eng.* **2019**, *44*, 7173–7185. [CrossRef]
5. Zhou, L.; Zhang, Y.; Lin, X.; Li, C.; Cai, Z.; Yang, P. Optimal sizing of PV and BESS for a smart household considering different price mechanisms. *IEEE Access* **2018**, *6*, 41050–41059. [CrossRef]
6. Espina, E.; Llanos, J.; Burgos-Mellado, C.; Cárdenas-Dobson, R.; Martínez-Gómez, M.; Sáez, D. Distributed control strategies for microgrids: An overview. *IEEE Access* **2020**, *8*, 193412–193448. [CrossRef]
7. Lopes, J.A.P.; Moreira, C.L.; Madureira, A.G. Defining control strategies for microgrids islanded operation. *IEEE Trans. Power Syst.* **2006**, *21*, 916–924. [CrossRef]
8. Wang, H.; Fang, H.; Yu, X.; Liang, S. How real time pricing modifies chinese households' electricity consumption. *J. Clean. Prod.* **2018**, *178*, 776–790. [CrossRef]
9. Renfang, L.; Luping, S.; Sidai, G. The stepwise pricing mechanism research of residents' living power. *Energy Procedia* **2011**, *5*, 1371–1376. [CrossRef]
10. Dai, Y.; Gao, Y.; Gao, H.; Zhu, H. Real-time pricing scheme based on stackelberg game in smart grid with multiple power retailers. *Neurocomputing* **2017**, *260*, 149–156. [CrossRef]
11. Dragičević, T.; Lu, X.; Vasquez, J.C.; Guerrero, J.M. DC microgrids—Part I: A review of control strategies and stabilization techniques. *IEEE Trans. Power Electron.* **2016**, *31*, 4876–4891.
12. Habibullah, A.F.; Padhilah, F.A.; Kim, K.-H. Decentralized control of DC microgrid based on droop and voltage controls with electricity price consideration. *Sustainability* **2021**, *13*, 11398. [CrossRef]
13. Padhilah, F.A.; Kim, K.-H. A power flow control strategy for hybrid control architecture of DC microgrid under unreliable grid connection considering electricity price constraint. *Sustainability* **2020**, *12*, 7628. [CrossRef]
14. Habibullah, A.F.; Kim, K.-H. Decentralized power management of DC microgrid based on adaptive droop control with constant voltage regulation. *IEEE Access* **2022**, *10*, 129490–129504. [CrossRef]
15. Mehdi, M.; Kim, C.H.; Saad, M. Robust centralized control for dc islanded microgrid considering communication network delay. *IEEE Access* **2020**, *8*, 77765–77778. [CrossRef]
16. Dehkordi, N.M.; Sadati, N.; Hamzeh, M. Distributed robust finite-time secondary voltage and frequency control of islanded microgrids. *IEEE Trans. Power Syst.* **2017**, *32*, 3648–3659. [CrossRef]
17. Li, X.; Jiang, W.; Wang, J.; Wang, P.; Wu, X. An autonomous control scheme of global smooth transitions for bidirectional DC-DC converter in DC microgrid. *IEEE Trans. Energy Convers.* **2021**, *36*, 950–960. [CrossRef]
18. Li, J.; Liu, Y.; Wu, L. Optimal operation for community-based multi-party microgrid in grid-connected and islanded modes. *IEEE Trans. Smart Grid* **2018**, *9*, 756–765. [CrossRef]
19. Xia, Y.; Wei, W.; Peng, Y.; Yang, P.; Yu, M. Decentralized coordination control for parallel bidirectional power converters in a grid-connected DC microgrid. *IEEE Trans. Smart Grid* **2018**, *9*, 6850–6861. [CrossRef]
20. Dragicevic, T.; Wu, D.; Shafiee, Q.; Meng, L. Distributed and decentralized control architectures for converter-interfaced microgrids. *Chin. J. Electr. Eng.* **2017**, *3*, 41–52.

21. Shirkhani, M.; Tavoosi, J.; Danyali, S.; Sarvenoee, A.K.; Abdali, A.; Mohammadzadeh, A.; Zhang, C. A review on microgrid decentralized energy/voltage control structures and methods. *Energy Rep.* **2023**, *10*, 368–380. [CrossRef]
22. Li, Z.; Shahidehpour, M.; Aminifar, F. Cybersecurity in distributed power systems. *Proc. IEEE* **2017**, *105*, 1367–1388. [CrossRef]
23. Gu, Y.; Xiang, X.; Li, W.; He, X. Mode-adaptive decentralized control for renewable dc microgrid with enhanced reliability and flexibility. *IEEE Trans. Power Electron.* **2014**, *29*, 5072–5080. [CrossRef]
24. Guerrero, J.M.; Vasquez, J.C.; Matas, J.; De Vicuña, L.G.; Castilla, M. Hierarchical control of droop-controlled AC and DC microgrids—A general approach toward standardization. *IEEE Trans. Ind. Electron.* **2010**, *58*, 158–172. [CrossRef]
25. Xu, Q.; Xiao, J.; Hu, X.; Wang, P.; Lee, M.Y. A decentralized power management strategy for hybrid energy storage system with autonomous bus voltage restoration and state-of-charge recovery. *IEEE Trans. Ind. Electron.* **2017**, *64*, 7098–7108. [CrossRef]
26. Tuckey, A.; Zabihi, S.; Round, S. Decentralized control of a microgrid. In Proceedings of the 19th European Conference on Power Electronics and Applications, Warsaw, Poland, 11–14 September 2017.
27. Khorsandi, A.; Ashourloo, M.; Mokhtari, H. A decentralized control method for a low-voltage DC microgrid. *IEEE Trans. Energy Convers.* **2014**, *29*, 793–801. [CrossRef]
28. Gao, F.; Kang, R.; Cao, J.; Yang, T. Primary and secondary control in DC microgrids: A review. *J. Mod. Power Syst. Clean Energy.* **2019**, *7*, 227–242. [CrossRef]
29. Nguyen, T.V.; Kim, K.-H. Power flow control strategy and reliable DC-link voltage restoration for DC microgrid under grid fault conditions. *Sustainability* **2019**, *11*, 3781. [CrossRef]
30. Yu, Y.; Liu, G.-P.; Huang, Y.; Guerrero, J.M. Distributed data-driven secondary regulation for the conflict between voltage recovery and accurate current sharing in DC microgrids. *IEEE Trans. Power Electron.* **2023**, *38*, 9617–9634. [CrossRef]
31. Dogger, J.D.; Roossien, B.; Nieuwenhout, F.D.J. Characterization of li-ion batteries for intelligent management of distributed grid-connected storage. *IEEE Trans. Energy Convers.* **2010**, *26*, 256–263. [CrossRef]
32. Ayodele, T.R.; Ogunjuyigbe, A.S.O.; Akpeji, K.O.; Akinola, O.O. Prioritized rule based load management technique for residential building powered by PV/battery system. *Eng. Sci. Technol. Int. J.* **2017**, *20*, 859–873. [CrossRef]
33. Xu, Y.; Liu, C.-C.; Schneider, K.P.; Tuffner, F.K.; Ton, D.T. Microgrids for service restoration to critical load in a resilient distribution system. *IEEE Trans. Smart Grid* **2016**, *9*, 426–437. [CrossRef]
34. Gao, H.; Chen, Y.; Xu, Y.; Liu, C.-C. Resilience-oriented critical load restoration using microgrids in distribution systems. *IEEE Trans. Smart Grid* **2016**, *7*, 2837–2848. [CrossRef]